REPORT DOCUMENTATION PAGE

Form Approved OMB NO. 0704-0188

1. REPORT DATE (DD-MM-YYYY)	2. REPORT TYPE	3. DATES COVERED (From - To)
26-04-2021	Final Report	1-May-2015 - 31-Dec-2020

4. TITLE AND SUBTITLE

Final Report: New Routes for Structural, Orbital, and Magnetic Control in Isovalent Oxide Superlattices within 6.1.1 Strong Correlations and Novel Quantum Phases of Matter

5a. CONTRACT NUMBER
W911NF-15-1-0133

5b. GRANT NUMBER

5c. PROGRAM ELEMENT NUMBER
611102

6. AUTHORS

5d. PROJECT NUMBER

5e. TASK NUMBER

5f. WORK UNIT NUMBER

7. PERFORMING ORGANIZATION NAMES AND ADDRESSES

Drexel University
Office of Research
3201 Arch Street, Suite 100
Philadelphia, PA 19104 -2875

8. PERFORMING ORGANIZATION REPORT NUMBER

9. SPONSORING/MONITORING AGENCY NAME(S) AND ADDRESS (ES)

U.S. Army Research Office
P.O. Box 12211
Research Triangle Park, NC 27709-2211

10. SPONSOR/MONITOR'S ACRONYM(S)
ARO

11. SPONSOR/MONITOR'S REPORT NUMBER(S)
66981-EL.14

12. DISTRIBUTION AVAILIBILITY STATEMENT

Approved for public release; distribution is unlimited.

13. SUPPLEMENTARY NOTES

The views, opinions and/or findings contained in this report are those of the author(s) and should not contrued as an official Department of the Army position, policy or decision, unless so designated by other documentation.

14. ABSTRACT

15. SUBJECT TERMS

16. SECURITY CLASSIFICATION OF:			17. LIMITATION OF ABSTRACT	15. NUMBER OF PAGES	19a. NAME OF RESPONSIBLE PERSON
a. REPORT	b. ABSTRACT	c. THIS PAGE			Steven May
UU	UU	UU	UU		19b. TELEPHONE NUMBER 215-571-3650

RPPR Final Report
as of 21-May-2021

Agency Code: 21XD

Proposal Number: 66981EL **Agreement Number: W911NF-15-1-0133**
INVESTIGATOR(S):

Name: Steven Joseph May
Email: sjm95@drexel.edu
Phone Number: 2155713650
Principal: Y

Organization: **Drexel University**
Address: Office of Research, Philadelphia, PA 191042875
Country: USA
DUNS Number: 002604817 EIN: 231352630

Report Date: 31-Mar-2021 Date Received: 26-Apr-2021
Final Report for Period Beginning 01-May-2015 and Ending 31-Dec-2020
Title: New Routes for Structural, Orbital, and Magnetic Control in Isovalent Oxide Superlattices within 6.1.1 Strong Correlations and Novel Quantum Phases of Matter
Begin Performance Period: 01-May-2015 **End Performance Period:** 31-Dec-2020
Report Term: 0-Other

Submitted By: Steven May Email: sjm95@drexel.edu
Phone: (215) 571-3650

Distribution Statement: 1-Approved for public release; distribution is unlimited.

STEM Degrees: **STEM Participants:** 2

Major Goals: This project aimed to discover novel physical phenomena in correlated ABO3 oxide superlattices by using interfacial coupling to control electronic degrees of freedom beyond the charge density, such as electronic bandwidth and orbital polarization (goals 1 - 3). The final year of the project focused on the study of interfaces in magnetic topological heterostructures (goal 4).
1. To demonstrate approaches for structural and orbital “delta-doping” as well as routes to more spatially confined electronic degree of freedom (beyond carrier density) in isovalent oxide superlattices.
2. To realize heterostructured materials with complex three-dimensional orbital ordering.
3. To develop new means to understand and control novel magnetotransport behavior arising from non-collinear spin textures, with emphasis on isovalent superlattices with spatially varying structural, orbital, and magnetic characteristics.
4. To use resonant x-ray scattering techniques in the study of magnetic topological heterostructures to provide quantitative and elementally-resolved measures of chemical intermixing, structural and magnetic roughness, and magnetization at buried interfaces with sub-nm spatial resolution.

Accomplishments: please see attached pdf file.

RPPR Final Report
as of 21-May-2021

Training Opportunities: The project provided partial support for PhD student Amanda Huon. She received her PhD in December 2018 and then took a postdoctoral research position at Oak Ridge National Laboratory. She recently accepted a tenure-track Physics faculty position at the University of the Sciences in Philadelphia. While supported by this project, she learned many experimental skills including thin film deposition, electrical and magnetic characterization, and neutron scattering.

The project provided full support to two postdoctoral researchers: Eun Ju Moon from 5/2015 to 8/2016, and Paul Rogge from 9/2016 to 2/2020. Dr. Moon is now an instrument scientist at SUNY Buffalo; Dr. Rogge is now an engineer at the IRS.

The project provided research opportunities to undergraduate students. Jared Gdanski worked on thin film deposition, graduated in 2020 and is now pursuing a PhD in physics from Ohio State University. Michael Barsoum worked on oxide superlattice growth and x-ray characterization during the summer after his first-year (second year of the project). Michael is graduating from materials science and engineering in 2021 and will pursue a PhD in materials from Northwestern University. Elliot Sayles worked on fitting the resonant x-ray reflectivity data during the summer of 2020 and is a student in the materials science and engineering department. Christopher Lee worked on oxide thin film deposition and optical characterization and graduated from Drexel with a degree in biology in 2019.

Results Dissemination: The project resulted in 14 peer reviewed publications (to date), 13 contributed presentations at conferences, and 22 invited presentations at conferences, workshops, and departmental seminars. Please see uploaded pdf file for a full list of publications and presentations resulting from this project.

Honors and Awards: The PI gave 22 invited talks on the research from this project, including 2 at the APS March Meeting (2018 and 2021).

During the course of this project, the PI was promoted from associate to full professor (2019) with the research accomplishments from this project playing an important role in that promotion. In summer 2020, the PI was promoted to department head.

In 2020, the PI was elected to a three-year term as Secretary/Treasurer for the Division of Materials Physics executive committee with APS.

The PI was selected in 2020 as an APS Outstanding Referee, an award officially bestowed in March 2021.

Protocol Activity Status:

Technology Transfer: Nothing to Report

PARTICIPANTS:

Participant Type: PD/PI
Participant: Steven May
Person Months Worked: 1.00 **Funding Support:**
Project Contribution:
National Academy Member: N

Participant Type: Graduate Student (research assistant)
Participant: Prajwal Laxmeesha
Person Months Worked: 5.00 **Funding Support:**
Project Contribution:
National Academy Member: N

Participant Type: Undergraduate Student

RPPR Final Report
as of 21-May-2021

Participant: Elliot Sayles
Person Months Worked: 1.00 **Funding Support:**
Project Contribution:
National Academy Member: N

ARTICLES:

Publication Type: Journal Article Peer Reviewed: Y **Publication Status:** 1-Published
Journal: Applied Physics Letters
Publication Identifier Type: DOI Publication Identifier: 10.1063/1.4932132
Volume: 1.07E+002 Issue: 1.4E+001 First Page #: 142901
Date Submitted: Date Published:
Publication Location:
Article Title: Electronic transition above room temperature in CaMn7O12 films
Authors:
Keywords: complex oxide heterostructures, electronic phase transitions, correlated electron systems
Abstract: We report on the electronic phase transition in CaMn7O12 quadruple perovskite films synthesized by oxide molecular beam epitaxy on SrLaAlO4 and La0.3Sr0.7Al0.65Ta0.35O3 substrates. We use x-ray diffraction and transmission electron microscopy to confirm that the CaMn7O12 phase has been realized. Temperature dependent resistivity measurements reveal a signature of a charge ordering phase transition at ┐425 K, consistent with bulk CaMn7O12. The transition temperature is found to be relatively invariant to changes in the cation stoichiometry. Density functional theory calculations reveal the changes in atomic and electronic structure induced by the charge ordering transition.
Distribution Statement: 3-Distribution authorized to U.S. Government Agencies and their contractors
Acknowledged Federal Support:

Publication Type: Journal Article Peer Reviewed: Y **Publication Status:** 1-Published
Journal: Advanced Functional Materials
Publication Identifier Type: DOI Publication Identifier: 10.1002/adfm.201505328
Volume: 26 Issue: 0 First Page #: 3118
Date Submitted: 5/9/17 12:00AM Date Published: 5/10/16 8:00AM
Publication Location:
Article Title: Synthesis and Characterization of 2D Molybdenum Carbide (MXene)
Authors: Joseph Halim, Sankalp Kota, Maria R. Lukatskaya, Michael Naguib, Meng-Qiang Zhao, Eun Ju Moon, J
Keywords: 2D materials, MXene, Mo2C
Abstract: Large scale synthesis and delamination of two-dimensional (2D) Mo2CTx (where T is a surface termination) has been achieved by selectively etching gallium from the recently discovered nanolaminated, ternary transition metal carbide Mo2Ga2C. Different synthesis and delamination routes result in different flake morphologies. The resistivity of Mo2CTx free-standing films increases by an order of magnitude as the temperature is reduced from 300 to 10 K in suggesting semiconductor-like behavior of this MXene, in contrast to Ti3C2Tx which exhibits metallic behavior. At 10 K, the magnetoresistance is positive. Additionally, changes in electronic transport are observed upon annealing of the films. When 2 ?m thick films are tested as electrodes in supercapacitors, capacitances as high as 700 F/cm3 in a 1 molar sulfuric acid electrolyte and high capacity retention for at least 10,000 cycles at 10 A/g are obtained. Freestanding films of Mo2CTx with ~8 wt. % carbon nanotubes perform well when teste
Distribution Statement: 3-Distribution authorized to U.S. Government Agencies and their contractors
Acknowledged Federal Support: **Y**

RPPR Final Report
as of 21-May-2021

Publication Type: Journal Article Peer Reviewed: Y **Publication Status:** 1-Published
Journal: Nanoscale Horizons
Publication Identifier Type: DOI Publication Identifier: 10.1039/C5NH00125K
Volume: 1 Issue: 3 First Page #: 227
Date Submitted: 8/24/16 12:00AM Date Published:
Publication Location:
Article Title: Control of electronic properties of 2D carbides (MXenes) by manipulating their transition metal layers
Authors: Babak Anasori, Chenyang Shi, Eun Ju Moon, Yu Xie, Cooper A. Voigt, Paul R. C. Kent, Steven J. May,
Keywords: MXene, 2D materials
Abstract: In this study, a transition from metallic to semiconducting-like behavior has been demonstrated in two-dimensional (2D) transition metal carbides by replacing titanium with molybdenum in the outer transition metal (M) layers of M3C2 and M4C3 MXenes. MXene structure consists of stacks of n+1 layers of M covering n layers of C or N in an [MX]nM arrangement. Recently, two new families of 2D double transition metal carbides MXenes were discovered, M'2M"C2 and M'2M"2C3 - where M' and M" are two different early transition metals, such as Mo, Cr, Ta, Nb, V, and Ti. M' atoms only occupy the outer layers and M" atoms fill the middle layers. In other words, M' atomic layers sandwich the middle M"-C layers. Using X-ray atomic pair distribution function (PDF) analysis on Mo2TiC2 and Mo2Ti2C3 MXenes, we present the first quantitative analysis of structures of these novel materials and experimentally confirm that Mo atoms are in the outer layers of the [MC]nM structures.
Distribution Statement: 3-Distribution authorized to U.S. Government Agencies and their contractors
Acknowledged Federal Support: **Y**

Publication Type: Journal Article Peer Reviewed: Y **Publication Status:** 1-Published
Journal: Physical Review B
Publication Identifier Type: DOI Publication Identifier: 10.1103/PhysRevB.95.155135
Volume: 95 Issue: 15 First Page #: 155135
Date Submitted: 5/9/17 12:00AM Date Published: 4/1/17 4:00AM
Publication Location:
Article Title: Growth and electrical transport properties of La0.7Sr0.3MnO3 thin films on Sr2IrO4 single crystals
Authors: E. J. Moon, A. F. May, P. Shafer, E. Arenholz, S. J. May
Keywords: correlated electron systems, oxide heterostructures
Abstract: We report the physical properties of La0.7Sr0.3MnO3 thin films on Sr2IrO4 single crystals. The manganite films are deposited using oxide molecular beam epitaxy on flux-grown (001)-oriented iridate crystals. Temperature-dependent magnetotransport and x-ray magnetic circular dichroism measurements reveal the presence of a ferromagnetic metallic ground state in the films, consistent with films grown on SrTiO3 and La0.3Sr0.7Al0.65Ta0.35O3. A parallel resistance model is used to separate conduction effects within the Sr2IrO4 substrate and the La0.7Sr0.3MnO3 thin films, revealing that the measured resistance maximum does not correspond to the manganite Curie temperature but results from a convolution of properties of the near-insulating substrate and metallic film. The ability to grow and characterize epitaxial perovskites on Sr2IrO4 crystals enables a new route for studying magnetism at oxide interfaces in the presence of strong spin-orbit interactions.
Distribution Statement: 3-Distribution authorized to U.S. Government Agencies and their contractors
Acknowledged Federal Support: **Y**

RPPR Final Report
as of 21-May-2021

Publication Type: Journal Article Peer Reviewed: Y **Publication Status:** 1-Published
Journal: Physical Review Letters
Publication Identifier Type: DOI Publication Identifier: 10.1103/PhysRevLett.119.197204
Volume: 119 Issue: First Page #: 197204
Date Submitted: 11/15/17 12:00AM Date Published: 11/10/17 5:00AM
Publication Location:
Article Title: Structural “Delta-Doping” to Control Local Magnetization in Isovalent Oxide Heterostructures
Authors: Eun Ju Moon, Qian He, Saurabh Ghosh, Brian J. Kirby, Sokrates T. Pantelides, Albina Y. Borisevich, St
Keywords: oxide heterostructures, octahedral rotations, correlated electron systems, delta-doping
Abstract: Delta-doping strategies, in which atomically thin layers of charged dopants are precisely deposited within a heterostructures, have played enabling roles in the discovery of new physical behavior in electronic materials. Here, we demonstrate a purely structural "delta-doping" strategy in complex oxide heterostructures, in which atomically thin manganite layers are inserted into an isovalent manganite host thereby modifying the local rotations of corner-connected MnO6 octahedra. Combining scanning transmission electron microscopy, polarized neutron reflectometry, and density functional theory, we reveal how local magnetic exchange interactions are enhanced within the spatially confined regions of suppressed octahedral rotations. The combined experimental and theoretical results illustrate the potential to utilize non-charge-based approaches to "doping" in order to enhance or suppress functional properties within spatially confined regions of oxide heterostructures.
Distribution Statement: 3-Distribution authorized to U.S. Government Agencies and their contractors
Acknowledged Federal Support: **Y**

Publication Type: Journal Article Peer Reviewed: Y **Publication Status:** 1-Published
Journal: APL Materials
Publication Identifier Type: DOI Publication Identifier: 10.1063/1.4994089
Volume: 5 Issue: First Page #: 096105
Date Submitted: 11/15/17 12:00AM Date Published: 9/18/17 4:00AM
Publication Location:
Article Title: Effect of Chemical Pressure on the Electronic Phase Transition in Ca1-xSrxMn7O12 Films
Authors: A. Huon, D.Lee, A. Herklotz, M. R. Fitzsimmons, H. N. Lee, and S. J. May
Keywords: correlated oxides, perovskites, manganites
Abstract: We demonstrate how chemical pressure affects the structural and electronic phase transitions of the quadruple perovskite CaMn7O12 by Sr doping, a compound that exhibits a charge ordering transition above room temperature making it a candidate for oxide electronics. We have synthesized Ca1-xSrxMn7O12 ($0 < x < 0.6$) thin films by oxide molecular beam epitaxy on (LaAlO3)0.3(SrAl0.5Ta0.5O3)0.7 (LSAT) substrates. The substitution of Sr for Ca results in a linear expansion of the lattice, as revealed by X-ray diffraction. Temperature-dependent resistivity and X-ray diffraction measurements are used to demonstrate that the coupled charge-ordering and structural phase transitions can be tuned with Sr doping. An increase in Sr concentration acts to decrease the phase transition temperature (T*) from 426 K at $x = 0$ to 385 K at $x = 0.6$. The presence of a tunable electronic phase transition, above room temperature, points to the potential applicability in sensors or oxide electronics.
Distribution Statement: 3-Distribution authorized to U.S. Government Agencies and their contractors
Acknowledged Federal Support: **Y**

RPPR Final Report
as of 21-May-2021

Publication Type: Journal Article Peer Reviewed: Y **Publication Status:** 1-Published
Journal: Physical Review Materials
Publication Identifier Type: DOI Publication Identifier: 10.1103/PhysRevMaterials.2.015002
Volume: 2 Issue: First Page #: 015002
Date Submitted: 8/29/18 12:00AM Date Published: 1/30/18 5:00AM
Publication Location:
Article Title: The electronic structure of negative charge transfer CaFeO3 across the metal-insulator transition
Authors: P. C. Rogge, R. U. Chandrasena, A. Cammarata, R. J. Green, P. Shafer, B. M. Lefler, A. Huon, A. Arab,
Keywords: correlated electron systems, oxide heterostructures, metal-insulator transitions, quantum materials
Abstract: We investigated the metal-insulator transition for epitaxial thin films of the perovskite CaFeO3, a material with a significant oxygen ligand hole contribution to its electronic structure. We find that biaxial tensile and compressive strain suppress the metal-insulator transition temperature. By combining hard X-ray photoelectron spectroscopy, soft X-ray absorption spectroscopy, and density functional calculations, we resolve the element-specific changes to the electronic structure across the metal-insulator transition. We demonstrate that the Fe electron valence undergoes no observable change between the metallic and insulating states, whereas the O electronic configuration undergoes significant changes. This strongly supports the bond-disproportionation model of the metal-insulator transition for CaFeO3 and highlights the importance of ligand holes in its electronic structure.
Distribution Statement: 3-Distribution authorized to U.S. Government Agencies and their contractors
Acknowledged Federal Support: **Y**

Publication Type: Journal Article Peer Reviewed: Y **Publication Status:** 1-Published
Journal: Physical Review B
Publication Identifier Type: DOI Publication Identifier: 10.1103/PhysRevB.98.224419
Volume: 98 Issue: First Page #: 224419
Date Submitted: 2/21/19 12:00AM Date Published: 12/19/18 10:00AM
Publication Location:
Article Title: Helical magnetism in Sr-doped CaMn7O12 films
Authors: Amanda Huon, Anuradha M. Vibhakar, Alexander J. Grutter, Julie A. Borchers, Steven Disseler, Yaohua
Keywords: correlated oxides, spin textures, helical magnetism
Abstract: Noncollinear magnetism can play an important role in multiferroic materials but is relatively understudied in oxide heterostructures compared to their bulk counterparts. Using magnetometry and neutron diffraction, we demonstrate the presence of helical magnetic ordering in CaMn7O12 and Ca1-xSrxMn7O12 (for x up to 0.51) thin films. Consistent with bulk Ca1-xSrxMn7O12, the net magnetization increases with Sr doping. Neutron diffraction confirms that the helical magnetic structure remains incommensurate at all values of x, while the fundamental magnetic wavevector increases upon Sr substitution. This result demonstrates a chemical-based approach for tuning helical magnetism in quadruple perovskite films and enables future studies of strain and interfacial effects on helimagnetism in oxide heterostructures.
Distribution Statement: 3-Distribution authorized to U.S. Government Agencies and their contractors
Acknowledged Federal Support: **Y**

RPPR Final Report
as of 21-May-2021

Publication Type: Journal Article Peer Reviewed: Y **Publication Status:** 1-Published
Journal: Physical Review B
Publication Identifier Type: DOI Publication Identifier: 10.1103/PhysRevB.98.201115
Volume: 98 Issue: First Page #: 201115(R)
Date Submitted: 2/21/19 12:00AM Date Published: 11/28/18 5:00AM
Publication Location:
Article Title: Inverted orbital polarization in strained correlated oxide films
Authors: Paul C. Rogge, Robert J. Green, Padraic Shafer, Gilberto Fabbris, Andi M. Barbour, Benjamin M. Lefler,
Keywords: orbital polarization, correlated oxides, quantum heterostructures
Abstract: Manipulating the orbital occupation of valence electrons via epitaxial strain in an effort to induce new functional properties requires considerations of how changes in the local bonding environment affect the band structure at the Fermi level. Using synchrotron radiation to measure the x-ray linear dichroism of epitaxially strained films of the correlated oxide CaFeO3, we demonstrate that the orbital polarization of the Fe valence electrons is opposite from conventional understanding. Although the energetic ordering of the Fe 3d orbitals is confirmed by multiplet ligand field theory analysis to be consistent with previously reported strain-induced behavior, we find that the nominally higher energy orbital is more populated than the lower. We ascribe this inverted orbital polarization to an anisotropic bandwidth response to strain in a compound with nearly filled bands.
Distribution Statement: 3-Distribution authorized to U.S. Government Agencies and their contractors
Acknowledged Federal Support: **Y**

Publication Type: Journal Article Peer Reviewed: Y **Publication Status:** 1-Published
Journal: Physical Review Materials
Publication Identifier Type: DOI Publication Identifier: 10.1103/PhysRevMaterials.2.094402
Volume: 2 Issue: 9 First Page #: 094402
Date Submitted: 9/12/18 12:00AM Date Published: 9/1/18 4:00AM
Publication Location:
Article Title: Strain-induced competition between ferromagnetism and emergent antiferromagnetism in (Eu,Sr)
Authors: A. J. Grutter, S. M. Disseler, E. J. Moon, D. A. Gilbert, E. Arenholz, A. Suter, T. Prokscha, Z. Salman, B.
Keywords: correlated oxide heterostructures, magnetism
Abstract: We demonstrate emergent antiferromagnetic interactions in strained thin films of the mixed valence manganite (Eu,Sr)MnO3. Although the composition studied, Eu0.7Sr0.3MnO3, will nominally yield a ferromagnetic phase in the bulk, we observe significant suppression of the saturation magnetization in films under both tensile and compressive strain. Despite the magnetization suppression, muon spin rotation spectrometry and polarized neutron reflectometry reveal uniform magnetic ordering in these films. Neutron diffraction and x-ray absorption spectroscopy demonstrate high-temperature G-type antiferromagnetic order in films under tensile strain, in contrast to the A- and C-type orders that are found in the phase diagrams of bulk (Eu,Sr)MnO3 and other mixed-valence manganites. These probes also show that compressive strain results in a uniform but suppressed magnetization suggestive of moment canting resulting from competition between ferromagnetism and antiferromagnetism.
Distribution Statement: 3-Distribution authorized to U.S. Government Agencies and their contractors
Acknowledged Federal Support: **Y**

RPPR Final Report
as of 21-May-2021

Publication Type: Journal Article Peer Reviewed: Y **Publication Status:** 1-Published
Journal: Nature Communications
Publication Identifier Type: DOI Publication Identifier: 10.1038/s41467-018-06503-8
Volume: 9 Issue: 1 First Page #: 4034
Date Submitted: 10/17/18 12:00AM Date Published: 10/1/18 4:00AM
Publication Location:
Article Title: Tailoring manganese oxide with atomic precision to increase surface site availability for oxygen reduction catalysis
Authors: C. John Eom, Ding-Yuan Kuo, Carolina Adamo, Eun Ju Moon, Steve J. May, Ethan J. Crumlin, Darrell G
Keywords: oxide heterostructures, catalysis, perovskite oxides
Abstract: Controlling the structure of catalysts at the atomic level provides an opportunity to establish detailed understanding of the catalytic form-to-function and realize new, non-equilibrium catalytic structures. Here, advanced thin-film deposition is used to control the atomic structure of La2/3Sr1/3MnO3, a well-known catalyst for the oxygen reduction reaction. The surface and sub-surface is customized, whereas the overall composition and d-electron configuration of the oxide is kept constant. Although the addition of SrMnO3 benefits the oxygen reduction reaction via electronic structure and conductivity improvements, SrMnO3 can react with ambient air to reduce the surface site availability. Placing SrMnO3 in the subsurface underneath a LaMnO3 overlayer allows the catalyst to maintain the surface site availability while benefiting from improved electronic effects.
Distribution Statement: 3-Distribution authorized to U.S. Government Agencies and their contractors
Acknowledged Federal Support: **Y**

Publication Type: Journal Article Peer Reviewed: Y **Publication Status:** 1-Published
Journal: Advanced Materials
Publication Identifier Type: DOI Publication Identifier: 10.1002/adma.201902364
Volume: 31 Issue: First Page #: 1902364
Date Submitted: 11/18/20 12:00AM Date Published:
Publication Location:
Article Title: Depth-resolved modulation of metal-oxygen hybridization and orbital polarization across correlated oxide interfaces
Authors: Paul C. Rogge, Padraic Shafer, Gilberto Fabbris, Wen Hu, Elke Arenholz, Evgeunia Karapetrova, Mark I
Keywords: correlated oxide, band hybridization, resonant scattering
Abstract: Interface-induced modifications of the electronic, magnetic, and lattice degrees of freedom drive an array of novel physical properties in oxide heterostructures. Here large changes in metal-oxygen band hybridization, as measured in the oxygen ligand hole density, are induced as a result of interfacing two isovalent correlated oxides. Using resonant x-ray reflectivity, a superlattice of SrFeO3 and CaFeO3 is shown to exhibit an electronic character that spatially evolves from strongly O-like in SrFeO3 to strongly Fe-like in CaFeO3. This alternating degree of Fe electronic character is correlated with a modulation of an Fe 3d orbital polarization, giving rise to an orbital superstructure. At the SrFeO3/CaFeO3 interfaces, the ligand hole density and orbital polarization reconstruct in a single unit cell of CaFeO3, demonstrating how the mismatch in these electronic parameters is accommodated at the interface.
Distribution Statement: 1-Approved for public release; distribution is unlimited.
Acknowledged Federal Support: **Y**

RPPR Final Report
as of 21-May-2021

Partners

,

I certify that the information in the report is complete and accurate:
Signature: Steven May
Signature Date: 4/26/21 4:04PM

New Routes for Structural, Orbital, and Magnetic Control in Isovalent Oxide Superlattices
Final Technical Report
W911NF-15-1-0133
PI: Steven May (Drexel University)

Period of Performance: 5/1/2015 – 12/31/2020

Project Goals

This project aimed to discover novel physical phenomena in correlated ABO_3 oxide superlattices by using interfacial coupling to control electronic degrees of freedom beyond the charge density, such as electronic bandwidth and orbital polarization (goals 1 - 3). The final year of the project focused on the study of interfaces in magnetic topological heterostructures (goal 4).

1. To demonstrate approaches for structural and orbital "delta-doping" as well as routes to more spatially confined electronic degree of freedom (beyond carrier density) in isovalent oxide superlattices.
2. To realize heterostructured materials with complex three-dimensional orbital ordering.
3. To develop new means to understand and control novel magnetotransport behavior arising from non-collinear spin textures, with emphasis on isovalent superlattices with spatially varying structural, orbital, and magnetic characteristics.
4. To use resonant x-ray scattering techniques in the study of magnetic topological heterostructures to provide quantitative and elementally-resolved measures of chemical intermixing, structural and magnetic roughness, and magnetization at buried interfaces with sub-nm spatial resolution.

Summary of Accomplishments

- Provided the first demonstration of non-charge-based delta-doping by creating local confined regions of enhanced octahedral rotations in isovalent manganite superlattices. The structurally-doped regions exhibited increased magnetization and Curie temperatures compared to the surrounding host layers.
- Provided the first demonstration of spatially-modulated orbital polarization in which a non-zero e_g orbital polarization was established in four unit cells of $CaFeO_3$ adjoined to thicker $SrFeO_3$ layers. This is the first-time orbital delta-doping has been realized in a system with a nominally-uniform charge density.
- Discovered a new mechanism for interfacial reconstructions in oxide superlattices: an interfacial-induced alteration of the metal-oxygen hybridization as revealed through resonant soft x-ray reflectivity in isovalent ferrite superlattices.
- Provided evidence that a multi-q spin texture in $SrFeO_3$ is responsible for magnetotransport behavior, in contrast to $CaFeO_3$, where our scattering experiments suggest a single-q texture. We have also confirmed the presence of a spatially-modulated helical spin texture in $(Sr,Ca)Mn_7O_{12}$ films.
- Carried out the first resonant x-ray reflectivity measurements on magnetic topological heterostructures, providing evidence for a suppression of magnetization in Fe adjacent to Bi_2Se_3. These scattering experiments also provide many lessons learned about the future use of this technique to probe quantum material heterostructures.
- Published 14 papers, gave 22 invited talks, including at the APS March meeting, based on results from this project. Provided partial support to a female PhD student (Amanda Huon, who has accepted a faculty position for 2021 in the Physics Department at the University of the

Sciences in Philadelphia), a MS student (Prajwal Laxmeesha), and full support to 2 postdoctoral researchers (Eun Ju Moon and Paul Rogge).

Scientific Accomplishments

1. Structural delta-doping in manganite superlattices

The first major accomplishment of the project was the direct demonstration of structural delta-doping of ferromagnetism in $La_{0.5}Sr_{0.5}MnO_3$ (LSMO)/$La_{0.5}Ca_{0.5}MnO_3$ (LCMO) superlattices. Modulation and delta-doping strategies, in which atomically thin layers of charged dopants are precisely deposited within a heterostructures, have played enabling roles in the discovery of new physical behavior in electronic materials and in improving performance of electronic devices. While delta-doping has been extensively applied to semiconductors and oxides to alter local electronic densities, the importance of interrelated charge, lattice, and orbital degrees of freedom in correlated oxides points to non-charge-based local "doping" approaches that are not operative in conventional semiconductors.

The samples used for this aspect of the project were $(LSMO)_n/(LCMO)_{20}$ superlattices (n=2,4 unit cells) grown by molecular beam epitaxy. Both of the manganite layers are half-doped, so that the nominal Mn valence or charge density is uniform throughout the superlattice, thereby mitigating any potential effects of charge transfer and ensuring we are in a purely non-charge-based regime. Owing to its smaller tolerance factor, the octahedral rotations in LCMO are larger than those in LSMO and as a result the Curie temperature in bulk LCMO is ~250 K compared to ~350 K in LSMO. The central physical hypothesis was that the ultrathin LSMO layers will exhibit reduced octahedral rotations compared to the surrounding LCMO layers. This will create local regions of higher electronic bandwidth (carrier itinerancy) and thus enhanced magnetic exchange interactions and electronic conductivity within the delta-doped regions. We choose n=2 as the thinnest layer to test this idea as two *A*-site layers (La,SrO) are needed to fully enclose a MnO_6 octahedra.

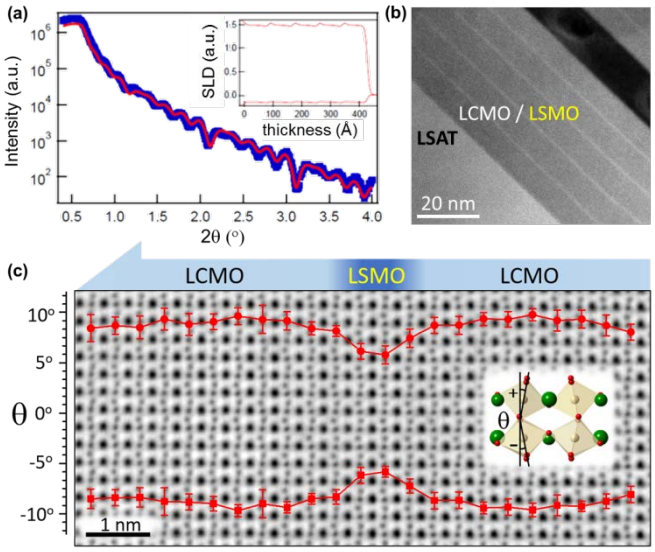

Figure 1. (a) X-ray reflectivity with obtained scattering length density profile inset; (b) scanning transmission electron microscopy image obtained by Qian He and Albina Borisevich. (c) Projected MnO_6 rotation angles (red symbols and line) overlaid on bright field STEM image showing the suppression of rotations within the two LSMO unit cells.

Structural characterization of the *n*=2 superlattice is shown in Figure 1. X-ray reflectivity [Fig. 1(a)] and scanning transmission electron microscopy (STEM) [Fig. 1(b)] confirm the presence of distinct LSMO and LCMO layers and verify the general $(LSMO)_2/(LCMO)_{20}$ composition of the sample. The projected octahedral rotation angle was mapped throughout the superlattice using bright-field imaging techniques. As shown in Figure 1(c), the rotation angle is suppressed within the two LSMO unit cells, confirming that the local atomic structure can be effectively "delta-doped".

In order to explore the physical effects of the structural delta-doping, polarized neutron reflectometry (PNR) measurements were performed as a function of temperature on both the n = 2 and 4 superlattices. PNR enables quantitative depth profiling of in-plane magnetization, allowing for the magnetism within the superlattice to be spatially resolved. The results for the *n*=2 superlattice are shown in Figure 2. We have obtained excellent fits to the reflectivity [Fig. 2(a)] and spin asymmetry [Fig. 2(b)]. The obtained magnetic depth profile [Fig. 2(c)] clearly reveals an enhanced magnetization within the LSMO layers compared to the surrounding LCMO layers at all temperatures. The enhanced magnetization is quite narrow in its spatial width, being confined to approximately the two LSMO unit cells. Note that the composition of the manganite layers ($La_{0.5}Sr_{0.5}MnO_3$ and $La_{0.5}Ca_{0.5}MnO_3$) is at half-doping, which marks the boundary between ferromagnetic and antiferromagnetic phases in bulk. Numerous studies have shown that small changes in doping produce dramatic changes to the magnetic properties at this region of the phase diagram. We have also attempted to fit the PNR data to a variety of other potential physical scenarios (decreased M in LSMO, uniform M throughout the superlattice, etc), but alternative models do not reproduce the basic features of the PNR data. Averaging over all the LSMO and LCMO layers, the temperature dependent magnetization of the LSMO and LCMO is plotted in Figure 2(d). Through extrapolation, the Curie temperature of the ultrathin LSMO layers is clearly higher than that of the thicker LCMO layer. This is also consistent with enhanced electronic bandwidth due to the structural delta-doping leading to increased local ferromagnetic exchange interactions within the LSMO. Similar PNR results were also obtained on the *n*=4 superlattice, confirming that the enhanced local magnetization from structural delta-doping is reproducible.

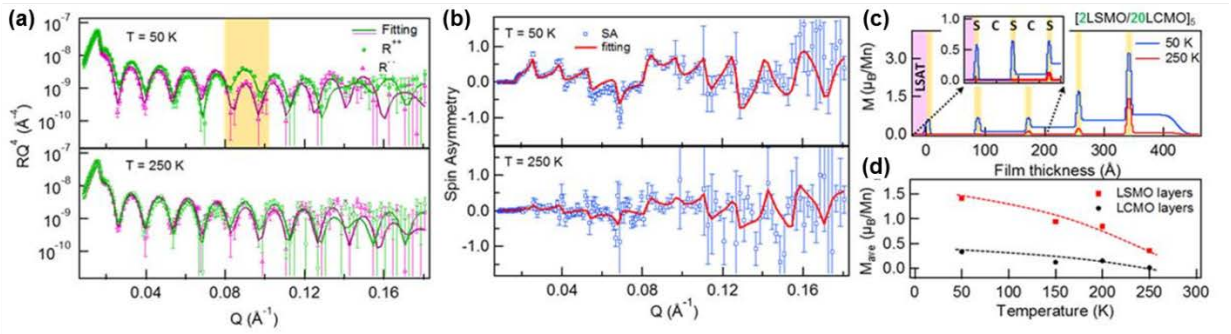

Figure 2. (a) Polarized neutron reflectivity data and fits (solid lines) measured at 50 and 250 K; (b) the corresponding fits to the spin asymmetry, defined as the difference in R^+ and R^- over the total reflectivity. (c) The obtained magnetic depth profile conclusively demonstrates that the magnetization is enhanced within the LSMO layers which exhibit reduced octahedral rotations but the same Mn valence as the LCMO layers. (d) The average magnetization within the LSMO and LCMO layers as a function of temperature is indicative of a higher Curie temperature within the 2 unit cell LSMO layers compared to the 20 unit cell LCMO layers.

This work was published in *Physical Review Letters* [PRL **119**, 197204 (2017)] and was selected as a highlight in the 2018 NIST Center for Neutron Research annual report (https://doi.org/10.6028/NIST.SP.1231). The ability to spatially confine magnetic states without altering the local charge density offers a new strategy for studying magnetism in the ultrathin two-dimensional limit. While previous efforts to understand magnetism in the two-dimensional regime have largely focused on the study of ultrathin films, such investigations unavoidably introduce significant effects from the free surface or film/substrate interface. The demonstrated structural delta-doping keeps the three-dimensional nature of the ABO_3 perovskite crystal intact while systematically altering ordering temperatures of buried magnetic layers. Similarly, metal-insulator and charge ordering transitions are dependent on *B*-O-*B* bond angles, allowing for the potential confinement of such electronic phase transitions through the local doping of octahedral rotations. Therefore, this approach is broadly applicable for understanding and controlling magnetism or electronic phases as a function of confinement and dimensionality.

2. Confined orbital polarization and hybridization interfacial reconstruction in ferrite superlattices

The second major accomplishment of the project was the demonstration of confined e_g orbital polarization and an interfacial reconstruction of metal-oxygen hybridization in isovalent ferrite superlattices. These effects were measured in a $[(CaFeO_3)_5/(SrFeO_3)_{20}]x4$ superlattice grown by molecular beam epitaxy. From a purely ionic standpoint, both $SrFeO_3$ and $CaFeO_3$ should exhibit e_g^1 (d^4) electronic configurations, which is an electron count that can host orbital polarization (occupancy of the two e_g orbitals, x^2-y^2 and z^2-r^2, can differ). However, due to the energetic unfavorability of a pure Fe^{4+} oxidation state and the strong covalency between Fe and O, these compounds are known to host holes derived from oxygen states (so-called ligand holes, denoted by $\underline{L}$). Therefore, the actual electronic configuration is best described by as a mixture of $d^4\underline{L}^0$ and $d^5\underline{L}^1$. The weight of each configuration is set by the band hybridization or covalency: a greater degree of hybridization leads to more $d^5\underline{L}^1$, while a more ionic (less hybridized) bond results in more $d^4\underline{L}^0$. Critically, a $d^4\underline{L}^0$ configuration can exhibit e_g orbital polarization while $d^5\underline{L}^1$ cannot. Therefore, we hypothesized that there would be a clear correlation between the degree of band hybridization and the magnitude of the orbital polarization. Through our analysis we were able to confirm the presence of a superstructure of both orbital

polarization and band hybridization within the nominally isovalent superlattice. We were also able to demonstrate an interfacial reconstruction of the band hybridization or degree of metal-oxygen covalency at a correlated oxide interface.

The superlattice structure was confirmed by measuring the off-resonance reflectivity at 800 eV and then simulating the reflectivity using the non-resonant scattering factors. X-ray reflectivity was measured at different soft x-ray wavelengths at the Advanced Light Source, Beamline 4.0.2, and at the National Synchrotron Light Source-II, Beamline 23-ID-1. The reflectivity was simulated using the ReMagX software package. The off-resonant reflectivity exhibits short period oscillations associated with the total film thickness, as well as q_{00l} Bragg peaks that are consistent with a periodic structure of the $SrFeO_3/CaFeO_3$ repeat unit (**Fig. 3**). The suppressed intensity of q_{005} is consistent with the 4:1 ratio of the $SrFeO_3$:$CaFeO_3$ thicknesses: For a superstructure of uniform subunits with thickness m and n, the structure factor of the (m/n + 1) Bragg reflection is strongly suppressed. To quantify the thickness of the individual $CaFeO_3$ and $SrFeO_3$ layers and the interfacial roughness, the reflectivity was simulated and compared to experiment. The best fit was obtained with uniform thicknesses of nominally 20 $SrFeO_3$ unit cells and 5 $CaFeO_3$ unit cells. The interlayer roughness is approximately 2 Å, indicating excellent film quality. The optimized structure includes a top 3 Å thick layer of SrO. Hard x-ray diffraction measurements indicated that the heterostructure is relaxed from the substrate, with the thinner $CaFeO_3$ layers instead strained to the thicker $SrFeO_3$ layers such that $CaFeO_3$ is under moderate tensile strain (~1.6%).

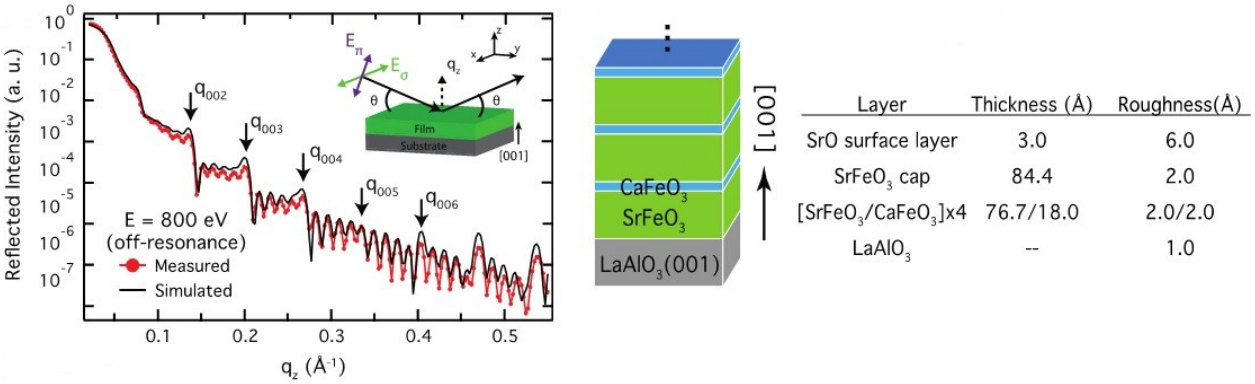

Layer	Thickness (Å)	Roughness(Å)
SrO surface layer	3.0	6.0
$SrFeO_3$ cap	84.4	2.0
$[SrFeO_3/CaFeO_3]$x4	76.7/18.0	2.0/2.0
$LaAlO_3$	--	1.0

Figure 3. (left) Off-resonant x-ray reflectivity of the $[(SrFeO_3)_{20}/(CaFeO_3)_5]$x4 superlattice on $LaAlO_3$ (001). The superlattice Bragg q_{00l} reflections are labeled; the inset schematic shows the x-ray polarizations used for the linear dichroism measurements. (right) Schematic of the superlattice structure. The table shows the film parameters resulting from the reflectivity simulation.

To probe the Fe-O hybridization as a function of depth, we measured resonant soft x-ray reflectivity near the O *K*-edge. The spectroscopic signature of oxygen ligand holes ($\underline{L}$) is a prepeak feature in the O *K*-edge x-ray absorption, and the prepeak intensity is proportional to the ligand hole density. As seen in Figure 4(a), the O *K*-edge x-ray absorption of individual, monolithic films of $CaFeO_3$ and $SrFeO_3$ exhibit a prepeak at 526-529 eV. We note that both prepeak intensities for the data presented in Figure 2(a) are suppressed compared to bulk as this data was collected using the surface-sensitive total electron yield technique and there is partial oxygen loss at the film surface. Nonetheless, the presence of the prepeak is clearly observed in $SrFeO_3$ and $CaFeO_3$, which both host the nominal Fe^{4+} state, and is not present in a control sample of $EuFeO_3$ (Fe^{3+}, pure $d^5\underline{L}^0$) that is shown for comparison.

In Figure 4(b), the reflectivity measured with the photon energy tuned to the oxygen prepeak feature (528.5 eV) and to the nominal O *K*-edge (530.1 eV, herein referred to as the O *K* edge, is presented, which reveals two observations. First, the prepeak reflectivity exhibits more intense

superlattice reflections compared to the O *K*-edge reflectivity. Because the intensity of a Bragg reflection is proportional to the square of the difference of the energy-dependent scattering factors for the sublayers within the superlattice cell, which to first order corresponds to a difference in the effective electron density for $SrFeO_3$ and $CaFeO_3$, this indicates that the $CaFeO_3$ and $SrFeO_3$ layers have a much larger difference in their O prepeak scattering factors than their O *K*-edge scattering factors, which we attribute to different ligand hole densities between the $SrFeO_3$ and $CaFeO_3$ layers. This is unexpected because previous work has estimated comparable ligand hole densities (~0.9 ligand holes per formula unit) for $SrFeO_3$ and $CaFeO_3$. Thus, the sample exhibits a superstructure of modulated metal-oxygen hybridization. Second, in contrast to the O *K*-edge reflectivity, the prepeak reflectivity exhibits enhanced intensity at the forbidden q_{005} reflection, which indicates that the scattering factors of the interface differ from the interior. This is clear evidence for a reconstruction of the ligand hole density at the $SrFeO_3/CaFeO_3$ interface.

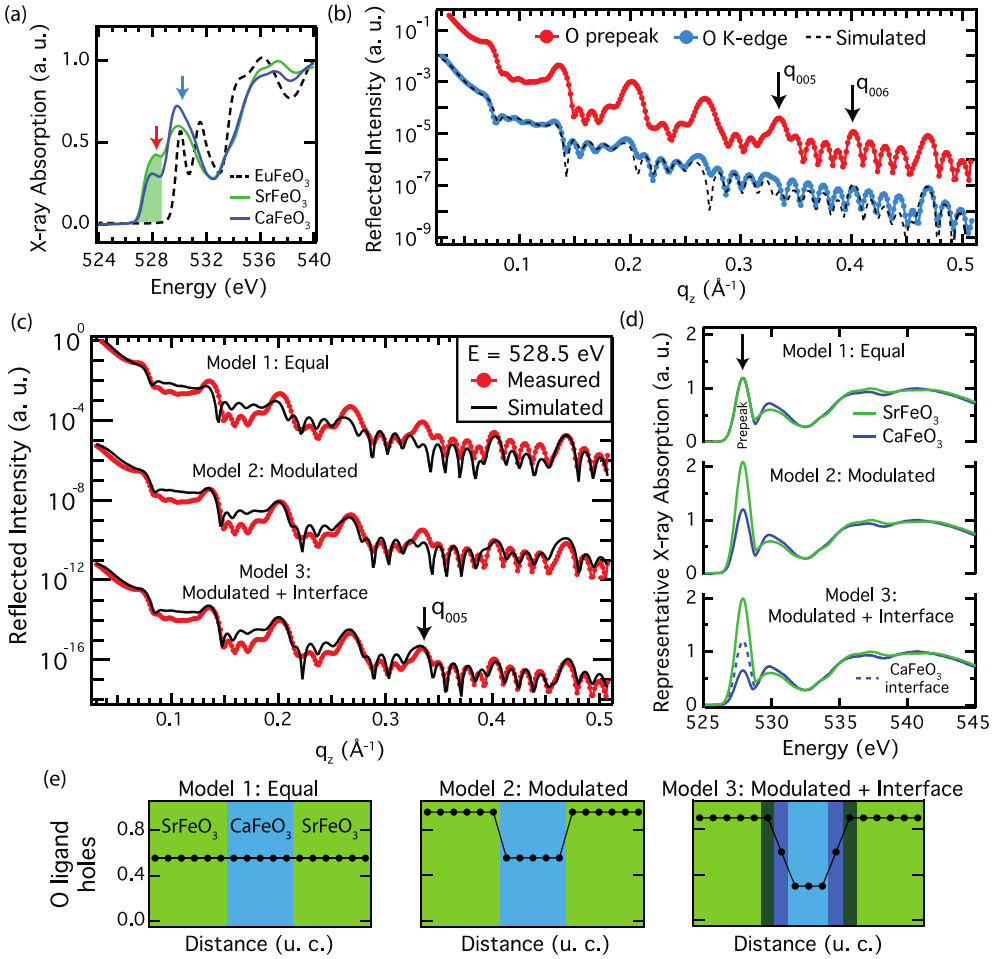

Figure 4. (a) X-ray absorption across the O *K*-edge for individual films with Fe^{3+} ($EuFeO_3$) and nominal Fe^{4+} ($SrFeO_3$ and $CaFeO_3$), which exhibit a prepeak feature (526-529 eV, shaded) due to strong Fe-O hybridization. Arrows denote energies at which the reflectivity was measured. (b) Resonant reflectivity measured at the O prepeak (528.5 eV, red) and at the O *K*-edge (530.1 eV, blue), along with the simulated reflectivity for the O *K*-edge (530.1 eV, dashed, black line). (c) Prepeak reflectivity for three simulated scenarios. (d) The representative x-ray absorption spectra with altered O prepeak intensities that produced the best reflectivity fit for each model in (c), where the $SrFeO_3$ prepeak intensity is comparable to that measured in bulk $SrFeO_3$. (e) The O ligand hole density as a function of distance across the $SrFeO_3/CaFeO_3$ interfaces in the superlattice for the different models. Each data point represents one unit cell. The interfacial regions in Model 3 are denoted by the additional shaded regions.

To further support this analysis, the resonant reflectivity was simulated by computing the resonant complex refractive indices for $SrFeO_3$ and $CaFeO_3$. Using the film structure determined from the off-resonant reflectivity, the reflectivity at the O *K*-edge resonance energy (530.1 eV) was simulated. As seen in Figure 4(b), excellent agreement is achieved without the use of fitting parameters, where the superlattice reflections are well-captured, including the suppressed q_{005} reflection at q_z = 0.330 Å^{-1}. Next, three scenarios for the prepeak reflectivity were simulated to determine the ligand hole concentration as a function of depth throughout the superlattice. As shown in Figure 4(c-e), the models consisted of: i) an equal ligand hole density for $SrFeO_3$ and $CaFeO_3$ (Model 1); ii) different ligand hole densities for $SrFeO_3$ and $CaFeO_3$ (Model 2); and iii) a 1 unit cell thick region within each $SrFeO_3$ and $CaFeO_3$ layer at each interface is allowed to be distinct from the layer interior (Model 3). In all scenarios, the structural parameters were fixed and the number of free parameters was minimized by constraining the optical parameters to be equal for all $SrFeO_3$ layers and all $CaFeO_3$ layers. To model potential differences in ligand hole densities, we varied the O prepeak x-ray absorption intensity of both $SrFeO_3$ and $CaFeO_3$ and re-computed the resonant refractive index, $n = 1 - \delta + i\beta$. The resulting relationship of δ and β at 528.5 eV (prepeak energy) as a function of the modified prepeak x-ray absorption intensity was obtained and input into the reflectivity simulation software, which varies the prepeak optical constants in order to determine the best fit. The prepeak x-ray absorption intensities for the $SrFeO_3$ and $CaFeO_3$ layers obtained from the best fit are plotted as the representative x-ray absorption spectra in Figure 4(d).

The simulations clearly reveal the presence of a modulated ligand hole density and an interfacial region – a single unit cell at the interface within the $CaFeO_3$ – that has a distinct prepeak intensity from the non-interfacial $SrFeO_3$ and $CaFeO_3$. As can be seen in Figure 4(c), the reflectivity that results from an equal ligand hole density (Model 1) does not reproduce the measured Bragg intensities. The presence of a modulated band hybridization (Model 2) does capture the Bragg intensities but does not yield the 005 Bragg reflection that is present in the measured reflectivity. The best fit is obtained using Model 3, where at each interface the ligand hole density of a 1-unit-cell thick region within the $SrFeO_3$ and $CaFeO_3$ layers is allowed to be distinct from the ligand hole density of their respective layer interior. As seen in Figure 4(c), the best fit is notably improved over Models 1 and 2, where the intensity of the forbidden q_{005} reflection is now replicated, and the agreement for $q_z >$ 0.3 Å^{-1} is additionally improved. In the best fit, the $CaFeO_3$ interior has a significantly lower ligand hole density than $SrFeO_3$ (~3x less), and the 1 unit cell $CaFeO_3$ interfacial regions exhibit an average between these two extremes. This is illustrated in Figure 4(d) by the significant difference in prepeak x-ray absorption intensities obtained from the best fit in Model 3. Simulations of other interfacial reconstructions (for example, using 2-unit-cell thick regions) produced poorer fits. These simulations therefore confirm a modulated electronic structure associated with Fe-O hybridization and reveal that the $CaFeO_3$ layers in this superlattice have a significantly lower ligand hole density than the $SrFeO_3$ layers, where the large prepeak x-ray absorption intensity obtained for $SrFeO_3$ in Model 3 is consistent with a bulk-like ligand hole density. Furthermore, the analysis demonstrates how the disparate degree of metal-oxygen hybridization is reconciled at the interface through a single unit cell of $CaFeO_3$, as highlighted in Figure 4(e).

To understand the impact on the e_g orbital polarization, resonant reflectivity measurements were performed at the Fe *L*-edge using linearly polarized photons. The polarization-dependent reflectivity measured at the Fe L_3 (708.9 eV and 709.4 eV) and L_2 edge (722.4 eV) is shown in Figure 5(a). Some initial insights can be provided by inspection of the data. First, whereas the off-resonant (800 eV) and oxygen resonant reflectivity (528.5 and 530.1 eV) exhibit enhanced intensity at the Bragg reflections, in comparison the Bragg reflections of the Fe resonance energies at 708.9 and 709.4 eV have reduced intensity. This indicates that the difference in scattering factors between $CaFeO_3$ and $SrFeO_3$ is small and thus the resonant scattering factors for $CaFeO_3$ and $SrFeO_3$ on the Fe *L*-edge are

nearly equal at these energies, as expected if both $CaFeO_3$ and $SrFeO_3$ have the same formal Fe^{4+} valence state. This supports the conclusion that the O ligand hole modulation is not due to oxygen vacancies, which would reduce the Fe valence and thus alter the Fe optical parameters. Second, the reflected intensity is polarization-dependent. The reflectivity measured with photons polarized perpendicular and parallel to the scattering plane, R_σ and R_π, respectively, exhibit a phase shift, due to the e_g orbital polarization.

To extract the layer-resolved orbital polarization, we simulated the polarization-dependent reflectivity arising from different orbital polarizations within the $SrFeO_3$ and $CaFeO_3$ layers using x-ray linear dichroism (XLD) spectra of monolithic $SrFeO_3$ and $CaFeO_3$ films that we had measured previously [Figure 5(b)]. The comparison between the simulation and measured data is best seen by plotting the asymmetry of the measured reflected intensity, $(R_\sigma - R_\pi)/(R_\sigma + R_\pi)$, which is a measure of the XLD magnitude as a function of q_z. The asymmetry exhibits large features that, consistent with the superlattice structure, repeat in q_z. We determine the orbital polarization by fitting the asymmetry at 708.9 eV and then observe the resulting asymmetry at the other two energies. Importantly, we enable the simulation software to vary the magnitude of the x-ray linear dichroism (the magnitude of the orbital polarization) in order to determine the best fit with experiment. Similar to our approach in fitting the ligand hole density, we considered three models: uniform polarization, modulated polarization, modulated polarization with interfacial reconstructions. The best fit, shown in Figure 5(c), was obtained using the third model, in which a small $d_{3z^2-r^2}$ polarization is present in $SrFeO_3$ and much larger $d_{3z^2-r^2}$ polarization is present in the $CaFeO_3$ layers. At the interface, the $CaFeO_3$ orbital polarization is reduced by ~40%. Because only d^4L^0 contributes to the measured orbital polarization, the reduced Fe orbital polarization within the $CaFeO_3$ interface region is consistent with the increased interfacial ligand hole density (see Model 3 in Figure 4(e)). These results confirm that the proposed orbital superstructure has been realized and further reveal how the disparate degrees of orbital polarization are accommodated at the interfaces.

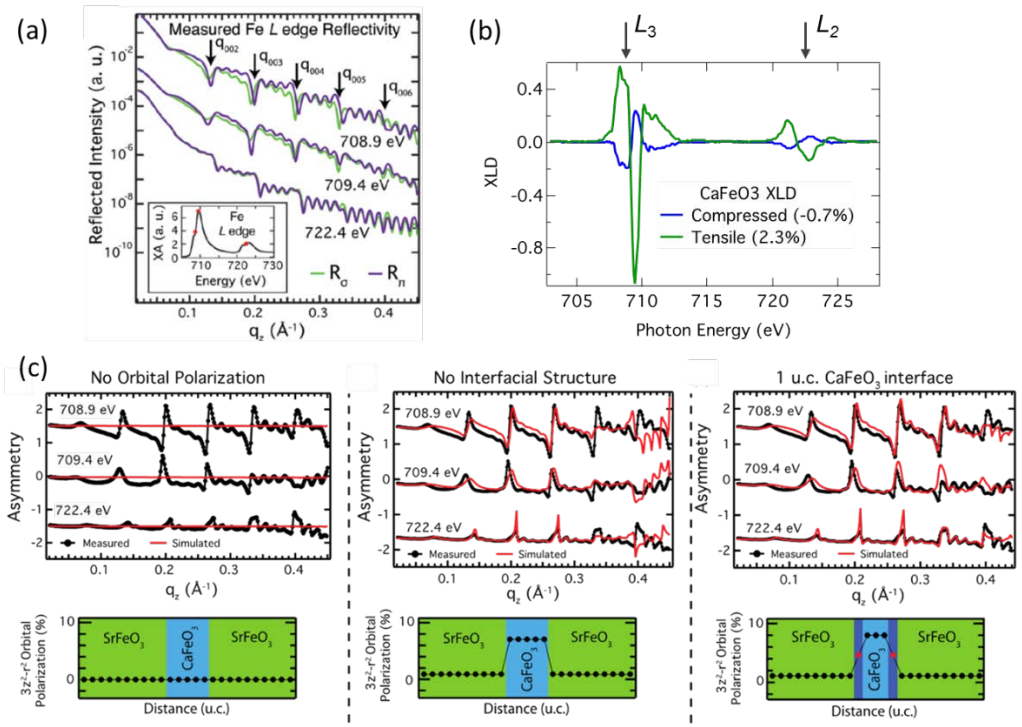

Figure 5. (a) Resonant reflectivity at the Fe *L*-edge measured with photons polarized perpendicular (R_σ) and parallel (R_π) to the scattering plane exhibits clear differences with photon polarization. Inset: Fe *L*-edge x-ray absorption spectra for $SrFeO_3$. (b) Measured XLD spectra for $CaFeO_3$ under tensile and compressive strain. (c) The reflectivity asymmetry, $(R_\sigma - R_\pi)/(R_\sigma + R_\pi)$, exhibits features that repeat in q_z in accordance with the film superstructure. The best fit with experiment is achieved when the $SrFeO_3$ layers have ~1% $d_{3z^2-r^2}$ polarization and the $CaFeO_3$ layers have ~8% $d_{3z^2-r^2}$ polarization that is reduced by approximately one-half within the 1 unit-cell-thick $CaFeO_3$ interfacial regions.

We have thus confirmed that isovalent correlated oxide superlattices host superstructures of both metal-oxygen hybridization and orbital polarization. This physical scenario is summarized in Figure 6. This is the first such report of this behavior and is a clear demonstration of a new mode of doping that alters the electronic orbital characterization instead of the carrier density. We believe this is the first time that resonant reflectivity has been used to depth profile band hybridization in heterostructures. The spatially varying Fe character additionally gives rise to an artificial Fe 3*d* orbital superstructure, also the first time such a ground state has been measured. This demonstration that metal-oxygen hybridization can be altered by and even reconstruct at oxide interfaces provides important context for understanding interfacial properties such as magnetism, superconductivity, and metal-insulator transitions which directly depend on ligand hole densities in metal oxides. This work was published in *Advanced Materials* [**31**, 1902364 (2019)] and formed the basis of an invited talk at the 2021 APS March Meeting.

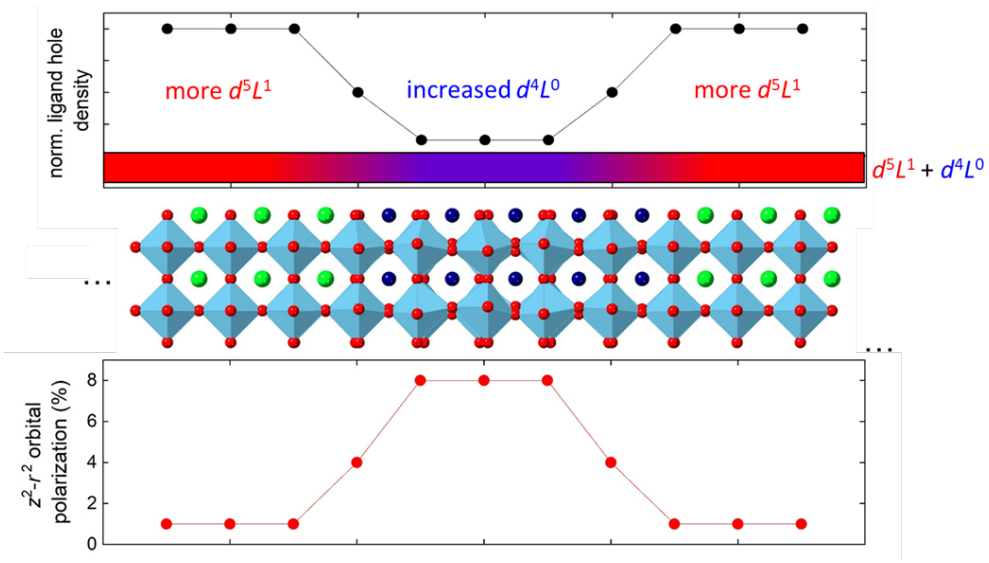

Figure 6. Schematic showing has the metal-oxygen hybridization as reflected in the ligand hole density and the orbital polarization evolve in concert across $SrFeO_3/CaFeO_3$ interfaces. The Ca atoms are represented by dark blue spheres, while the Sr atoms are represented by green spheres.

3. Non-collinear spin textures and magnetotransport

Interfacial and itinerancy dependence of multi-*q* spin textures in ($CaFeO_3$)/($SrFeO_3$) superlattices

A goal of the project was to explore magnetotransport phenomena in oxides with non-collinear spin textures. (Ca,Sr)FeO_3-based heterostructures are well suited for this area of pursuit given that both bulk $SrFeO_3$ and $CaFeO_3$ exhibit incommensurate helical magnetic order along the [111] direction. The metallic nature of $SrFeO_3$ enables high quality measurements of magnetoresistance as a probe of coupling between spin texture and electronic transport. This material system is particularly interesting as recent neutron scattering measurements [*PRB* **101**, 134406 (2020)] indicate that $SrFeO_3$ is not an incommensurate helical magnet that can be described by a single magnetic wavevector (single-*q*) but instead is a multi-*q* helical spin structure, analogous to a skyrmion lattice, a surprising result given that the Dzyaloshinskii-Moriya interaction is not operable in this cubic compound (the Fe-O-Fe does not break inversion symmetry). This leads to questions regarding the possible origin of the multi-*q* spin texture. Here we investigated the role that electron itineracy plays in this magnetic structure. In contrast to metallic $SrFeO_3$, $CaFeO_3$ is insulating in its magnetically ordered state, allowing the role of itineracy to be contrasted in the spin textures of these two materials that are otherwise very similar. We have also investigated magnetism in SrFeO3/CaFeO3 superlattices to understand how interfaces impact the non-collinear spin textures. This study has focused on magnetotransport measurements and resonant scattering experiments carried out in collaboration with Robert Green (University of Saskatchewan). The results below summarize the main results; more details can be found in our publication in *Physical Review Materials* [*PRM* **3**, 084404 (2019)].

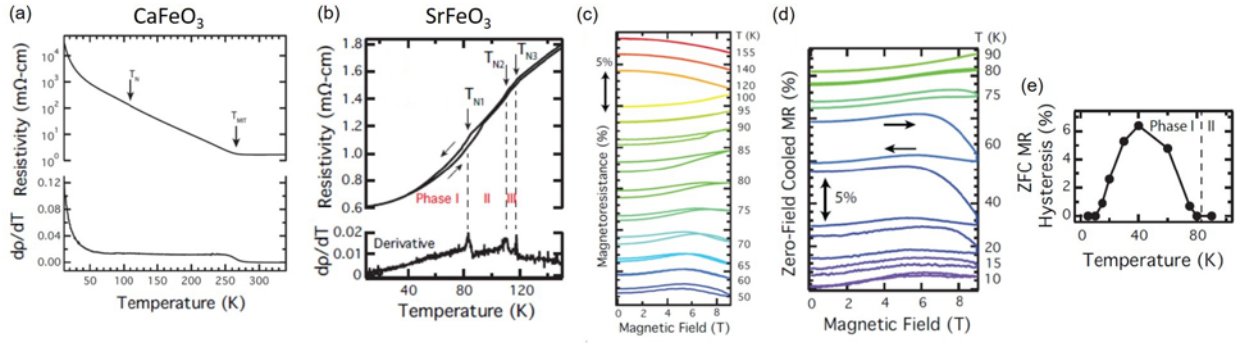

Figure 7. (a) Resistivity and the derivative of the log resistivity with respect to temperature in a $CaFeO_3$ film. In its helical magnetic state (below T_N), the film is an insulator with no anomalies in the resistivity upon magnetically ordering. (b) Resistivity and dρ/dT in a $SrFeO_3$ film. Three anomalies are present in the derivative, which correspond to the onset of the three distinct magnetic phases. (c) Magnetoresistance (MR) measured from $SrFeO_3$. The MR changes sign below 120 K, across the first magnetic transition. (d) Zero-field cooled MR, in which the sample was heated above T_N and recooled without a magnetic field for each of the MR data sets. (e) A hysteresis in the ZFC MR develops upon cooling through the Phase II to Phase I transition.

The temperature dependent resistivity of $CaFeO_3$ and $SrFeO_3$ films are shown in Figure 7(a,b). Consistent with bulk materials, the $CaFeO_3$ film exhibits a metal-insulator transition near 270 K and is well within the insulating state at its magnetic ordering temperature (T_N ~ 100 K). No anomalies are observed in the derivative of its resistivity. In contrast, $SrFeO_3$ is metallic with three anomalies present in its dρ/dT that have been assigned to the onset of three distinct magnetic phases [5]. The magnetoresistance (MR) measured in $SrFeO_3$ exhibits distinct behaviors within these different phases [Figure 7(c-e)]. The sign of the MR changes from negative to positive across the paramagnetic to Phase II/III magnetic transition. A hysteresis in the MR develops as the sample is cooled through the Phase II to Phase I transition. These results indicate a clear coupling of magnetotransport to changes in the spin texture within $SrFeO_3$.

Resonant x-ray diffraction was performed to better understand the spin structures within the $CaFeO_3$ and $SrFeO_3$ films. The magnetic Bragg peaks of $CaFeO_3$ and $SrFeO_3$ were measured at q ~ 0.46 $Å^{-1}$ and 0.36 $Å^{-1}$ along the H=K=L direction respectively, using a photon energy resonant with the Fe L_3-edge. These peaks correspond to incommensurate helices with periods of 17.5 Å ($SrFeO_3$) and 13.8 Å ($CaFeO_3$). As seen in Figure 8, the magnetic peaks increase in intensity with decreasing temperature. Integrating the peak area and plotting as a function of temperature in Fig. 8(c) reveals an onset of magnetic ordering at ~100 K for $CaFeO_3$, which is slightly suppressed compared to bulk (T_N = 120 K). The $SrFeO_3$ film has an onset temperature of ~115 K, which correlates with T_{N3} = 117 K as determined from the electrical transport data, and is similarly suppressed compared to bulk ($T_{N3,bulk}$ = 133 K).

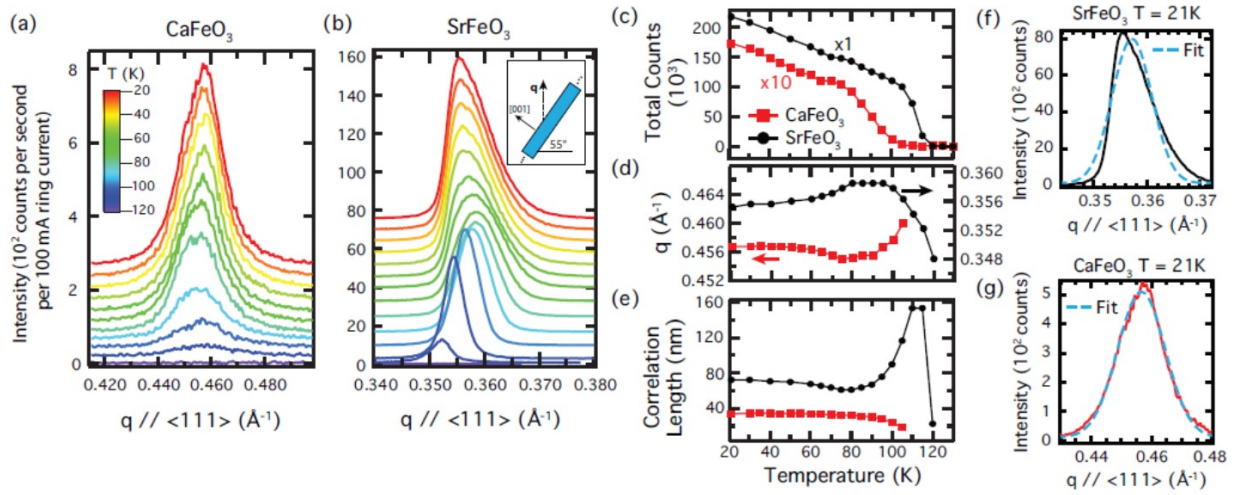

Figure 8. (a) Resonant magnetic scattering on the Fe *L*-edge along $q_{H=K=L}$ for the $CaFeO_3$ film and (b) the $SrFeO_3$ film. Data are offset in y. Inset in (b) shows the scattering geometry. (c) Total scattered intensity for the $CaFeO_3$ and $SrFeO_3$ films. (d) Magnitude of the scattering vector and (e) correlation length derived from the FWHM of the scattering peak. (f) Gaussian fit (dashed line) of the T = 21 K scattering peak (solid line) for $SrFeO_3$ and (g) $CaFeO_3$.

From the magnetic scattering data, the *q* vector as a function of temperature was extracted and is plotted in Fig. 8(d). Consistent with previous studies, the *q* vector in $SrFeO_3$ increases in magnitude with decreasing temperature, although we additionally observe a small decrease below 80 K (Phase II->I transition). In contrast, $CaFeO_3$ exhibits the opposite behavior, where the *q* vector decreases with decreasing temperature followed by a small increase at the lowest temperatures. Additionally, the overall change in *q* for $CaFeO_3$ is approximately 2x smaller than that exhibited by $SrFeO_3$. Comparing the peak shape evolution with temperature between $CaFeO_3$ and $SrFeO_3$ in Figs. 8(a,b), respectively, reveals three striking contrasts. First, $SrFeO_3$ exhibits a significantly enhanced scattering intensity compared to $CaFeO_3$. The second observable difference between $SrFeO_3$ and $CaFeO_3$ is whereas the $CaFeO_3$ peak is initially broad and becomes narrower with decreasing temperature, $SrFeO_3$ exhibits a narrow peak at the onset of helical ordering that then broadens with decreasing temperature. Converting the peak FWHM to a correlation length and plotting it as a function of temperature in Fig. 8(e) demonstrates that the $SrFeO_3$ correlation length is initially 4x greater than $CaFeO_3$ and nearly 2x greater at lower temperatures. The third major contrast between $SrFeO_3$ and $CaFeO_3$ is the significantly different peak shape evolution exhibited by $SrFeO_3$. With decreasing temperature, the peak asymmetrically broadens, where the expansion occurs at higher values of *q*, as highlighted in Fig. 8(f), where a symmetric Gaussian function cannot replicate the peak at 21 K. This broadening ceases below 80 K, which correlates with the previously determined Phase II->I transition in $SrFeO_3$ (T_{N1} = 83 K) extracted from electrical resistivity and ZFC MR measurements. In contrast, the $CaFeO_3$ scattering peak at 21 K is replicated by a symmetric Gaussian curve, as shown in Fig. 5(g), consistent with a single-*q* spin structure.

Recently, it has been proposed that $SrFeO_3$ supports multi-*q* magnetic structures such that the spin structure is a superposition of multiple *q* vectors along different crystallographic directions. Specifically, Phase II is proposed to be a single-domain quadruple-*q* structure consisting of proper screw helical ordering with propagation vectors along the four <111> vectors of the cubic unit cell [1]. The lack of hysteresis in the ZFC MR in Phase II is consistent with a single-domain structure. Additionally, the much larger domain size (correlation length) in Phase II $SrFeO_3$ compared to $CaFeO_3$ could arise from a single-domain structure, although we cannot rule out that the $CaFeO_3$ film may be

more defective than the $SrFeO_3$ film and thus has a smaller domain size. The source of the asymmetric change in peak shape and decreased correlation length exhibited by $SrFeO_3$ at lower temperatures is harder to disentangle with these data alone, but is consistent with the formation of a multi-*q* spin structure with a transition from Phase II->I. For instance, the peak broadening may arise from the transition from a quadruple-*q* single domain structure (Phase II) into a multidomain double-*q* structure where the two *q* vectors have a slightly different magnitude. This would result in the transition from a narrow peak (Phase II) to the asymmetric broadening (Phase I) that we have observed. Thus, these results, particularly the correlation length, highlight how x-ray scattering and magnetotransport measurements provide another way to probe multi-*q* magnetic states in heterostructures beyond neutron diffraction measurements.

These results provide important context for analyzing the $CaFeO_3$ scattering data. While previous studies have identified helical ordering in $CaFeO_3$, it is unknown if $CaFeO_3$ supports multi-*q* spin structures, which one may expect given its similarity to $SrFeO_3$. However, the data here demonstrate distinct differences between $SrFeO_3$ and $CaFeO_3$. The $CaFeO_3$ peak grows uniformly with decreasing temperature whereas the $SrFeO_3$ peak asymmetrically grows and exhibits larger changes in *q*. Additionally, the $CaFeO_3$ peak at low temperatures is symmetric, as seen in Fig. 8(g), suggesting that it does not replicate the presumed double-*q* ordering seen in $SrFeO_3$ at low temperatures. Although we cannot definitively determine the precise details of the spin structure within $CaFeO_3$, these results are consistent with a multi-domain, single-*q* helical structure, where different domains have helical ordering along one of the four <111> directions. A multi-domain helical state in $CaFeO_3$ is also consistent with the significantly reduced scattering intensity of $CaFeO_3$ compared to $SrFeO_3$; a 4x reduction would be expected given the 4 equivalent <111> directions. A possible reason for $SrFeO_3$ hosting multi-*q* spin textures but not $CaFeO_3$ is their different carrier itinerancies. Previous theoretical studies predict that single-*q* ordering can be destabilized in itinerant systems and instead multi-*q* structures are preferred. Here, neither lattice frustration nor the DM interaction is present in cubic $SrFeO_3$, thus leaving electron itinerancy as the likely source of multi-*q* states in $SrFeO_3$. The fact that $CaFeO_3$ is insulating below its Néel temperature further supports the conclusion that it has a simple single-*q* spin structure. Future magnetic field-dependent neutron diffraction measurements could confirm a single-*q* structure in $CaFeO_3$.

Additional evidence for different spin textures in $CaFeO_3$ and $SrFeO_3$ comes from resonant scattering data measured from $(CaFeO_3)_{20}/(SrFeO_3)_n$ superlattices. The magnetic scattering data obtained from $n = 1$, 4, and 6 superlattices are shown in Fig. 9(a). The *q* vector of all three superlattices is approximately equal to that of the monolithic $CaFeO_3$ film and the trend of the temperature dependent *q* vector resembles that of the $CaFeO_3$ film as well. The correlation length decreases with increasing $SrFeO_3$ thickness, indicating that the $SrFeO_3$ layers disrupt the helical ordering. At the lowest temperatures, the coherence length is 37 nm for the $n = 1$ superlattice and decreases to 16 nm for $n = 6$. For the $n = 1$ superlattice, the film thickness along [111] is 41 nm, and in the simple case in which the magnetic domains are isotropic, this would indicate that the helical ordering is coherent through the entire superlattice such that the magnetic moments in the $SrFeO_3$ layers are ordered coherently with those in the neighboring $CaFeO_3$ layers. For $n = 6$, the 16 nm correlation length is comparable to the thickness of the individual $CaFeO_3$ layers (~13 nm), indicating that the helical ordering within the $CaFeO_3$ layers does not propagate through the thicker $SrFeO_3$ layers. Propagation through $n = 1$ but not $n = 6$ offers further evidence that the helical spin structures of $SrFeO_3$ and $CaFeO_3$ are different (i.e., single-*q* vs multi-*q*). Given that both compounds exhibit helical ordering with comparable wavevectors, it is surprising that only 6 $SrFeO_3$ unit cells disrupts the helical ordering if the spin texture is that of a single-*q* helix. The coherence of the spin structure in the $n = 1$ superlattice implies that the multi-*q* spin texture of $SrFeO_3$ has been converted to a single-*q* texture due to proximity to $CaFeO_3$ and/or confinement effects.

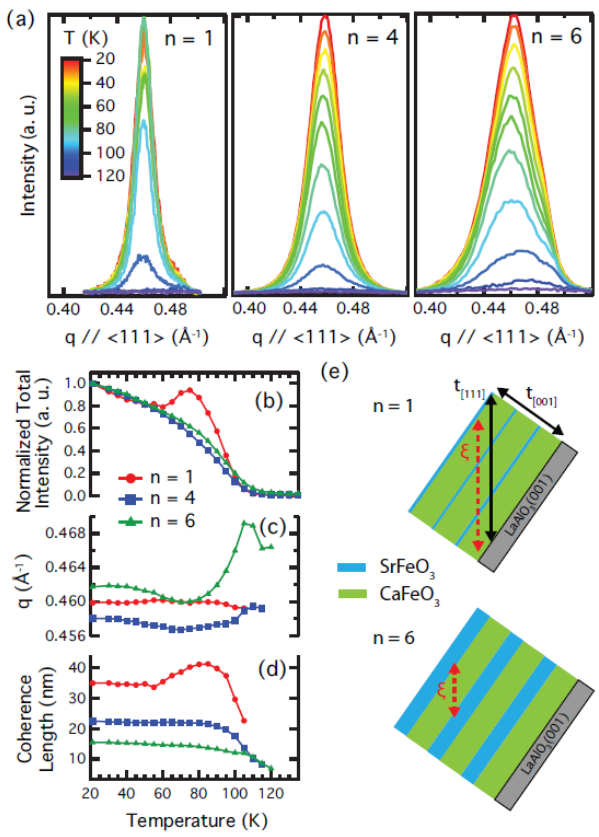

Figure 9. (a) Normalized resonant scattered intensity along $q_{H=K=L}$ for the three superlattices measured at different temperatures. (b) Total scattered intensity, (c) *q*, and (d) correlation length as a function of temperature. (e) Schematic of the superlattice structure in the angled measurement geometry and depictions of the measured correlation length relative to the relevant film dimensions for the *n* = 1 and 6 superlattices.

To summarize, this project has provided strong evidence that electron itinerancy plays a central role in the formation of differing non-collinear spin textures in metallic $SrFeO_3$ and insulating $CaFeO_3$, which in turned directly impacts magnetotransport behavior in these materials. We confirm that $SrFeO_3$ films exhibit magnetotransport signatures consistent with its previously determined multi-*q* magnetic structure, and further demonstrate that its resonant soft x-ray magnetic diffraction behavior with temperature is consistent with a multi-*q* spin structure. $CaFeO_3$, on the other hand, is found to exhibit significantly different magnetic diffraction characteristics compared to $SrFeO_3$, which we attribute to a single-*q* spin helix in $CaFeO_3$. Additionally, by synthesizing $CaFeO_3/SrFeO_3$ superlattices, we demonstrated that relatively thin layers (6 unit cells) of $SrFeO_3$ is sufficient to disrupt spin coherency through the superlattice, further supporting the conclusion that $SrFeO_3$ and $CaFeO_3$ have different helical magnetic structures. The lack of either Dzyaloshinskii-Moriya interaction or lattice frustration in cubic $SrFeO_3$, and the presence of only a single-*q* helical ordering in insulating $CaFeO_3$, supports the conclusion that electron itinerancy plays a critical role in the formation of the multi-*q* spin structures in $SrFeO_3$. Thus, tuning electron itinerancy in other non-collinear spin structures can potentially be a path towards controlling multi-*q* spin structures and their topologically non-trivial spin structures.

<u>Modulated helical spin textures in (Ca,Sr)Mn_7O_{12} films</u>

The non-collinear magnetic state of quadruple manganite perovskite films was also investigated. Using neutron diffraction, we confirmed the presence of helical magnetism within $Ca_{1-x}Sr_xMn_7O_{12}$ film and showed that the magnetic wavevector increases with increasing Sr concentration (increasing lattice volume). Below a second magnetic transition near 40 K, the helix becomes modulated with slightly differing angles between adjacent Mn spins. The state was confirmed through the presence of satellite reflections off of the primary magnetic *q*-vector. We believe this is the first time a modulated helical magnetic state has been measured in oxide thin films. This work was published in *Physical Review B* [**98**, 224419 (2018)].

4. Probing interfaces in magnetic topological heterostructures

Heterostructures with Bi_2Se_3/Fe ($Fe_{0.2}/Ni_{0.8}$) interfaces

The final year of the project shifted focus to applying resonant x-ray reflectivity to gain insights into the interfacial properties of topological heterostructures containing magnetic materials. This effort is focused on bilayers consisting of a topological insulator (Bi_2Se_3) and a ferromagnetic (FM) metal ($Ni_{0.81}Fe_{0.19}$ and Fe) that have been used in spin-transfer torque and spin pumping experiments. The heterostructures were synthesized at the 2DCC materials innovation platform user facility at Penn State University through a user proposal. Work focused on two samples: the first is a $Al_2O_3/Bi_2Se_3/Fe/AlO_x$ heterostructure in which all layers in the sample were deposited by MBE without breaking vacuum, the second is a $Al_2O_3/Bi_2Se_3/Fe_{0.2}Ni_{0.8}$/Ta heterostructure where the MBE-grown Bi_2Se_3 film was capped with an amorphous Se layer, then transferred through air to a sputtering chamber, in which the Se layer was removed and the ferromagnetic permalloy ($Fe_{0.2}Ni_{0.8}$) and Ta capping layers were deposited. In both samples, the Al_2O_3 is the substrate. Comparison between the two samples allows for a study of how synthesis conditions may impact interfacial magnetism between a ferromagnet and a topological insulator. Resonant x-ray reflectivity (RXR) experiments were performed at beamline 4.0.2 of the Advanced Light Source for the first sample and Sector 29-ID at the Advanced Photon Source for the second sample.

The fundamental approach with RXR measurements is to collect reflectivity data at many different photon energies, some of which are resonant with elemental electronic transitions. At these resonances, the atomic scattering factors are significantly enhanced leading to the contributions of different atoms within the heterostructures to play larger (or smaller) roles in the scattered signal at different energies. The resonant enhancement of the scattering factors (or optical constants, α and β) can be extracted from the x-ray absorption spectra. Data analysis involves simultaneously fitting the different reflectivity data sets to a single structural model to obtain a depth-profile of the atomic densities. While straightforward in principle, this process turns out to be exceedingly challenging in practice as relatively minor changes to the structural model can have significant impact on the simulated reflectivity data. As described in the year five progress report, simple models that use only a single layer to describe each individual material in the heterostructures do not yield any agreement between simulations and experimental data. As such, we have created models in which many of the materials (such as Fe) are broken into multiple layers. The Bi_2Se_3/Fe interface is modeled using multiple layers. Increasing the number of layers provides greater flexibility in the

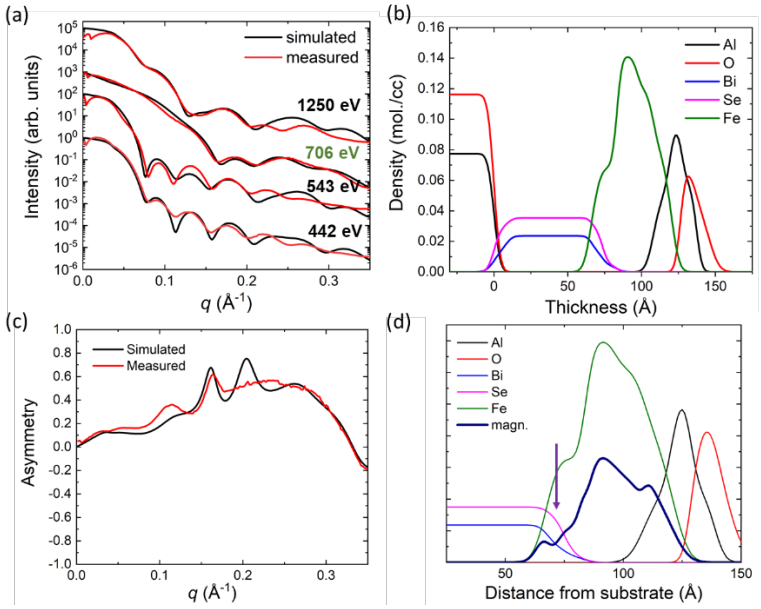

Figure 10. (a) Best fits to reflectivity data from the first sample at three off-resonant energies and at the Fe L-edge (706 eV). (b) The obtained elemental depth profile. (c) Best fit to the asymmetry data (difference between right and left circularly polarized reflectivity) measured at the Fe *L*-edge. (d) Obtained magnetization depth profile with magnetization shown as the thicker purple line.

structural model that can be obtained, but this also increases the number of fitting parameters, complexity of the model and time it takes to obtain a fit.

As the project focus was to understand interfacial magnetism, our strategy has been to find a fit that works well for the Fe *L*-edge resonance and is acceptable for the non-resonant energies. The year five progress report shows a structural model that works well for the non-resonant energies, but we were unable to get a good fit to the reflectivity data on the Fe resonance. Figure 10(a) shows the best fit data at two non-resonant energies, at the O *K*-edge (543 eV) and at the Fe *L*-edge (706 eV). The Fe *L*-edge fit is very good, while the other fits are in good agreement up to 0.2 $Å^{-1}$ and deviate at higher q values, suggesting some of the fine details (smaller length scale information contained at higher q) of the structural model are off but the basic structure is correct. The obtained structural model is shown in Figure 10(b).

The fit of the reflectivity asymmetry (which corresponds to the x-ray magnetic circular dichroism on the Fe *L*-edge) as a function of q is shown in Figure 10(c). The magnetization depth-profile throughout the Fe layer is presented in Figure 10(d). The magnetization largely follows the Fe density profile except near the Bi_2Se_3/Fe interface, where the magnetization is suppressed within the Fe over approximately 1 nm, highlighted by the pink arrow in Figure 10(d). We note that a similar suppressed interfacial magnetization was obtained in earlier versions of the refinements, suggesting that it is a physically significant feature of the heterostructure. This suppressed magnetization also coincides with a local reduction of the Fe density (the step-like feature in the Fe profile near the Bi_2Se_3/Fe interface) suggesting that either intermixing with the Bi_2Se_3 or roughness at the Bi_2Se_3/Fe junction plays an important role in the suppressed magnetization. There is a feature (local maxima) in the simulated asymmetry near q = 0.2 $Å^{-1}$ that shows up in all models that we have tested; we cannot remove this feature and its origin remains unknown.

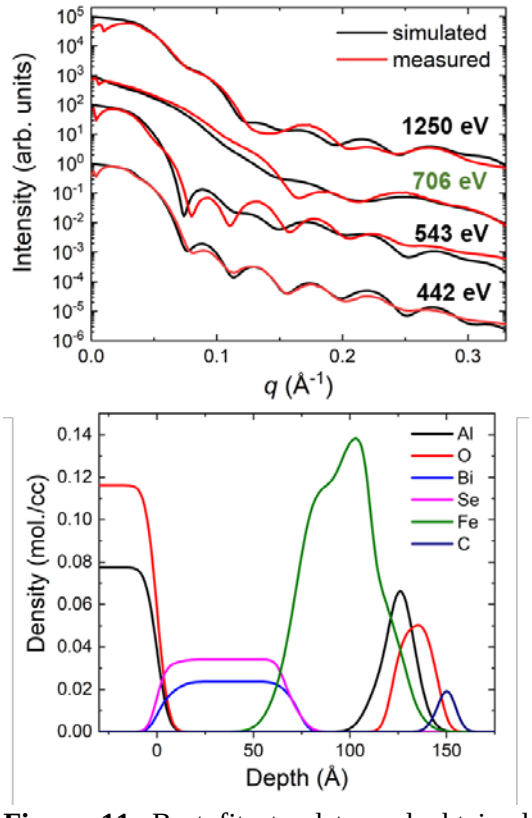

Figure 11. Best fits to date and obtained depth profile for model that includes a thin surface layer of naturally-occurring carbon (first sample).

While the period of performance has ended for the project, there is still one more avenue we are pursuing to improve the fits and ensure that our magnetic result is robust. The last set of models that we are trying involves adding a thin layer (< 1 nm) of carbon on the material surface, which would be a natural consequence of exposing a sample to air, a model detail that was recently suggested by a collaborator. To date, this has not improved the fits, the best of which are shown in Figure 11. The fit on the Fe resonance (706 eV), which contains a very similar Fe profile as the fit shown in Figure 10, also highlights how sensitive the resonant reflectivity is to subtle changes in the structural model.

Best fits to the second sample, the heterostructure that was transferred through air to a sputtering chamber for deposition of the ferromagnetic layer, are shown in Figure 12(a). Data collected at 1254 and 534 eV were fit, as were data collected at the Fe *L*-edge (723 eV) and Ni *L*-edge (873 eV). The Fe resonance data is well fit while the Ni resonance data has room for improvement in reproducing the data between q = 0.1 – 0.16 $Å^{-1}$. The resulting structural model [Fig. 12(b)] exhibits many expected features: an Al_2O_3/Bi_2Se_3

roughness that is similar to the first sample, oxidation of the Ta capping layer, and approximately 4:1 ratio of Ni/Fe in the permalloy layer.

However, the Bi_2Se_3/FM region differs between the two samples, as shown in Figure 12(c). The second sample, capped with Se and then transferred via air prior to sputtering the permalloy layer, exhibits a much larger roughness at this interface with an increased Se concentration at the topmost part of the Bi_2Se_3 layer compared to the first sample (Fe deposited directly on Bi_2Se_3 without breaking vacuum). This increased Se concentration is highlighted by the arrow in Fig. 12(c). The second sample also exhibits a much broader interfacial width within the ferromagnetic layer. We attribute these different interfacial profiles to the differences in deposition processes, with the all-MBE process yielding a less diffuse interface. We do not have a satisfactory fit to the magnetization for the second sample.

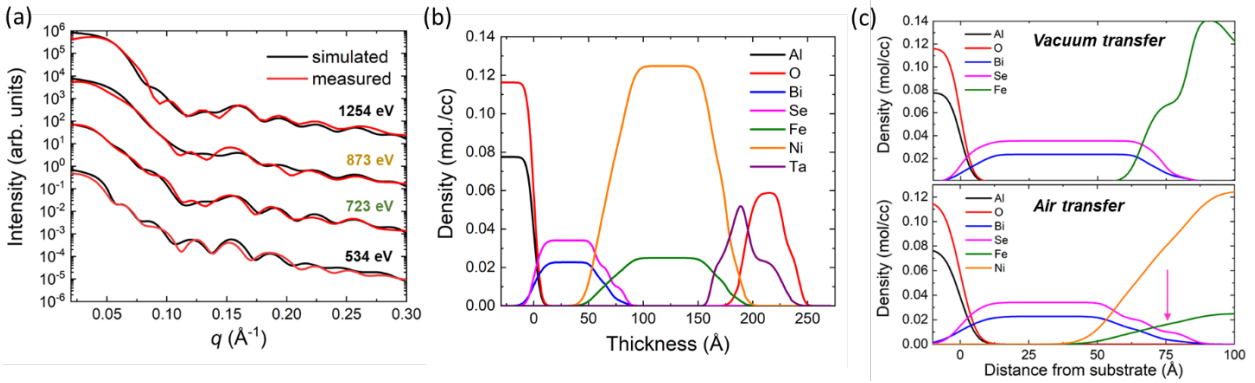

Figure 12. (a) Best fits to the reflectivity data from the second sample (the one transferred via air to a sputtering chamber for deposition of the $Fe_{0.2}Ni_{0.8}$/Ta layers). (b) The resulting elemental depth profile. (c) A comparison between the depth profiles of the Bi_2Se_3/FM interfaces for the two samples. The interface, especially the top of the Bi_2Se_3 layer, is more abrupt in the all-MBE sample (top) compared to the MBE+Sputtering sample (bottom). The air transferred sample was capped with Se before transfer to the sputtering system. The depth profile indicated an increased concentration of Se at the TI/FM interface, highlighted by the pink arrow.

<u>Trilayer ferromagnetic topological insulator structures</u>

We also carried out resonant x-ray reflectivity measurements on a $Cr_{0.3}Sb_{1.7}Te_3/Sb_2Te_3/V_{0.2}Sb_{1.8}Te_3/AlO_x$ trilayer structure provided by Cui-Zu Chang's group at Penn State. Measurements from this sample were motivated by the axion insulator state that was demonstrated in Cr-doped (Bi,Sb)Te_3/(Bi,Sb)Te_3/V-doped (Bi,Sb)Te_3 trilayer structures. The zero Hall conductance state, the signature of the axion insulator, is stabilized when the ferromagnetic Cr and V-doped layers have oppositely-aligned magnetization pointing out-of-the plane. When the magnetization of the two ferromagnetic layers is aligned, the structure enters the quantum anomalous Hall state. However, a quantitative layer-resolved understanding of the magnetization across the field-induced transition from these two states is lacking. The goal of this sub-effort was to use resonant soft x-ray reflectivity to map out the magnetization within the two ferromagnetic topological insulator layers through measurements on the Cr and V *L*-edges.

Resonant reflectivity data was collected from this sample at Sector 29-ID at the Advanced Photon Source, as shown in Figure 13. Measurements were performed at many off-resonant energies as well as on the V and Cr *L*-edges at 18 K, which is the base temperature for the beamline. However, the V *L*-edge was found to be very weak and did not result in a resonant enhancement. Additionally, there was very little circular dichroism on the V *L*-edge. This may be because the sample temperature was too close to the Curie temperature of the V-doped layer. Thus, these experiments were judged to not likely yield any useful physical insights.

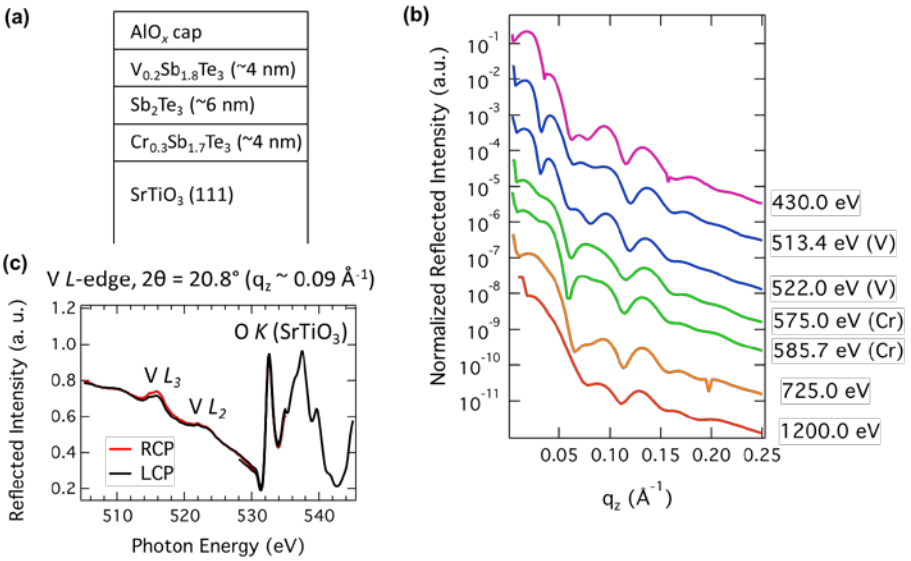

Figure 13. (a) Schematic of the trilayer heterostructures. (b) Reflectivity collected at a variety of off-resonant and resonant (V and Cr) conditions. (c) Reflectivity as a function of photon energy across the V *L*-edge and O *K*-edge. The absorption at the V *L*-edge is minimal, as is the circular dichroism. The O *K*-edge signal comes from the $SrTiO_3$ substrate.

Conclusions and Lessons Learned:

The work within the project using resonant reflectivity to probe magnetic topological heterostructures produced some direct conclusions about the interfacial behavior but also some lessons learned about moving forward with similar experiments in the future. These lessons are noted here as this technique had not yet been applied to topological insulator-based heterostructures and as such is at the forefront of characterization efforts of these systems.

1. RXR is able to produce elemental depth-profiles of topological heterostructures. This was most notable in the case of identifying the excess Se at the Bi_2Se_3/FM interface of the second sample. This result demonstrates the need for all layers to be deposited in a single vacuum chamber to produce the highest possible quality of interfaces.
2. The best fits indicate a suppression of magnetization within the Fe layer at the Bi_2Se_3/Fe interface. The suppressed magnetization coincides with interfacial roughness and thus it is not clear if the origin of the suppressed magnetization is extrinsic (due to intermixing or disorder) or is intrinsic (due to modification of the exchange energy within Fe at the interface with a topological insulator).
3. Obtaining good fits to all data sets is extremely challenging, for example, much more difficult than polarized neutron reflectivity, due to a few factors. First, the experiments produce a large amount of data, both in terms of reflectivity data sets at different energies and reflectivity data measured up to high q (can be up to 0.6 Å^{-1}). The large number of data sets requires simultaneously refining multiple sets to a single structural model. Fitting data beyond 0.4 Å^{-1} requires attention to increasingly small length scale features in the model (neutron reflectivity is typically measured to 0.15 Å^{-1} or less). This requires adding more layers and fitting parameters. Second, the optical constants are not fixed parameters (in contrast to neutron reflectivity) and instead are sensitive to ~0.1 eV changes in photon energy, when collecting data near a resonant transition. This adds a source of error as the optical constants must be extracted from x-ray absorption measurements and converted to α and β. As an experimenter, a central challenge is knowing when to stop fitting and deciding that the refinement is good enough even if all features in the data are not reproduced.

4. Recommendations for this approach in the future: There are paths toward simplifying or constraining the refinements. One option is to use superlattice samples [$(Bi_2Se_3)_n/(Fe)_m$] instead of bilayers. The superlattice will lead to Bragg peaks that can be fit more easily to extract interfacial information. I believe this was a key factor in the analysis from the ferrite superlattice producing better fits than the bilayer TI/FM samples. A second option would be to combine resonant x-ray reflectivity with polarized neutron reflectivity (PNR). PNR is not elementally resolved but it does provide a magnetization depth profile. This could be used to constrain modeling of the resonant magnetic x-ray reflectivity data and could therefore accelerate refinement of the RXR data. Similarly, cross-sectional STEM/EELS could be useful in constraining the elemental depth profiles, although STEM/EELS only probes a nanoscale area while x-ray scattering produces average information over a mm-sized area.
5. Despite the challenges, RXR is uniquely positioned to play an important role in characterization of topological heterostructures. It is non-destructive and could even be applied to measurement of patterned devices. It is quantitative in providing information on interfacial composition and elementally-resolved roughness. It can probe aspects of electronic character that are not accessible by STEM or neutron scattering, such as orbital information and potentially antiferromagnetism (using linear dichroism).

Project-Funded Publications

Research supported by this grant has been disseminated in the following publications:

1. A. Huon, A. C. Lang, D. Saldana-Greco, J. S. Lim, E. J. Moon, A. M. Rappe, M. L. Taheri, and S. J. May, "Electronic transition above room temperature in $CaMn_7O_{12}$ films", *Applied Physics Letters* **107**, 142901 (2015).
2. J. Halim, S. S. Kota, M. R. Lukatskaya, M. Naguib, M. Zhao, E. J. Moon, J. Pitock, J. Nanda, S. J. May, Y. Gogotsi, M. W. Barsoum, "Synthesis and Characterization of Two-Dimensional Molybdenum Carbide (MXene)", *Advanced Functional Materials* **26**, 3118 (2016).
3. B. Anasori, C. Shi, E. J. Moon, Y. Xie, C. A. Voigt, E. Dooryhee, P. R. C. Kent, S. J. May, S. J. L. Billinge, M. W. Barsoum, Y. Gogotsi, "Control of Electronic Properties of 2D Carbides (MXenes) by Manipulating Their Transition Metal Layers", *Nanoscale Horizons* **1**, 227 (2016).
4. E. J. Moon, A. F. May, P. Shafer, E. Arenholz, and S. J. May, "Growth and electrical transport properties of $La_{0.7}Sr_{0.3}MnO_3$ thin films on Sr_2IrO_4 single crystals", *Physical Review B* **95**, 155135 (2017).
5. A. Huon, D. Lee, A. Herklotz, M. R. Fitzsimmons, H. N. Lee and S. J. May, "Effects of Chemical Pressure on the Structural and Electronic Transport Properties in $Ca_{1-x}Sr_xMn_7O_{12}$", *APL Materials* **5**, 096105 (2017).
6. E. J. Moon, Q. He, S. Ghosh, B. J. Kirby, S. T. Pantelides, A. Y. Borisevich, and S. J. May, "Structural "δ Doping" to Control Local Magnetization in Isovalent Oxide Superlattices", *Physical Review Letters* **119**, 197204 (2017).
7. P. C. Rogge, R. U. Chandrasena, A. Cammarata, R. J. Green, P. Shafer, B. M. Lefler, A. Huon, A. Arab, E. Arenholz, H. N. Lee, T.-L. Lee, S. Nemšák, J. M. Rondinelli, A. X. Gray, and S. J. May, "Electronic structure of negative charge transfer $CaFeO_3$ across the metal-insulator transition", *Physical Review Materials* **2**, 015002 (2018).
8. A. J. Grutter, S. M. Disseler, E. J. Moon, D. A. Gilbert, E. Arenholz, A. Suter, T. Prokscha, Z. Salman, B. J. Kirby, and S. J. May, "Strain-Induced Competition between Ferromagnetism and Emergent Antiferromagnetism in $(Eu,Sr)MnO_3$", *Physical Review Materials* **2**, 094402 (2018).

9. C. J. Eom, D.-Y. Kuo, C. Adamo, E. J. Moon, S. J. May, E. J. Crumlin, D. G. Schlom, J. Suntivich, "Perovskite Manganese-Oxide Oxygen Reduction Catalysts Tailored with Atomic Precision to Increase Surface Site Availability", *Nature Communications* **9**, 4034 (2018).
10. P. C. Rogge, R. J. Green, P. Shafer, G. Fabbris, A. M. Barbour, B. M. Lefler, E. Arenholz, M. P. M. Dean, and S. J. May, "Inverted orbital polarization in strained correlated oxide films", *Physical Review B* **98**, 201115(R) (2018).
11. A. Huon, A. M. Vibhakar, A. J. Grutter, J. A. Borchers, S. Disseler, Y. Liu, W. Tian, F. Orlandi, P. Manuel, D. D. Khalyavin, Y. Sharma, A. Herklotz, H. N. Lee, M. R. Fitzsimmons, R. D. Johnson, and S. J. May, "Helical magnetism in Sr-doped $CaMn_7O_{12}$ films", *Physical Review B* **98**, 224419 (2018).
12. P. C. Rogge, R. J. Green, R. Sutarto, and S. J. May, "Itinerancy-dependent noncollinear spin textures in $SrFeO_3$, $CaFeO_3$, and $CaFeO_3/SrFeO_3$ heterostructures probed via resonant x-ray scattering", *Physical Review Materials* **3**, 084404 (2019).
13. W. Yang, R. U. Chandrasena, M. Gu, R. M. S. dos Reis, E. J. Moon, Arian Arab, M.-A. Husanu, J. Ciston, V. N. Strocov, J. M. Rondinelli, S. J. May, A. X. Gray, "Probing single unit-cell resolved electronic structure modulations in oxide superlattices with standing-wave photoemission", *Physical Review B* **100**, 125119 (2019).
14. P. C. Rogge, P. Shafer, G. Fabbris, W. Hu, E. Arenholz, E. Karapetrova, M. P. M. Dean, R. J. Green, S. J. May, "Depth-resolved modulation of metal-oxygen hybridization and orbital polarization across correlated oxide interfaces", *Advanced Materials* **31**, 1902364 (2019).

Project-Funded Conference Presentations

* denotes invited talk

The results from this project were presented at numerous invited departmental seminars given by the PI over the course of this reporting period. The ARO funding was acknowledged in all presentations.

1.* "Scattering approaches for characterizing octahedral rotations and their physical effects in oxide heterostructures", S. J. May, International Surface X-ray and Neutron Scattering Conference, Stony Brook, NY, July 10-14, 2016.
2.* "Structural approaches for controlling magnetism at complex oxide interfaces", S. J. May, Nanophases in Functional Materials workshop at the ALS User Meeting, Berkeley, CA, October 6-7, 2015.
3.* "Structural approaches for altering electronic and magnetic properties at manganite interfaces", S. J. May, Telluride Workshop on Competing Interactions and Colossal Responses in Transition Metal Compounds, Telluride, CO, June 8-12, 2015.
4.* "Engineering anion positions and compositions in perovskite oxide heterostructures" S. J. May, International Conference on Electroceramics, State College, PA, May 13 – 16, 2015.
5. "Enhanced magnetization in ultrathin manganite layers via structural delta-doping of octahedral rotations" Eun Ju Moon, B. J. Kirby, and S. J. May. American Physical Society March Meeting, Baltimore, MD, March 14-18, 2016.
6. "Electronic and magnetic properties of quadruple manganite $Ca_{1-x}Sr_xMn_7O_{12}$ films" Amanda Huon and S. J. May. American Physical Society March Meeting, Baltimore, MD, March 14-18, 2016.
7. "Electronic and Magnetic Properties of Epitaxial $Ca_{1-x}Sr_xMn_7O_{12}$ Films" A. Huon, A. Grutter, B. J. Kirby, and S. J. May. Materials Research Society Spring Meeting, Phoenix, March 29 – April 1, 2016.

8.* "Anion-based approaches to engineering functionality in perovskite oxide heterostructures", S. J. May, Brookhaven National Laboratory, Condensed Matter Physics and Materials Science seminar, January 26, 2017.
9.* "Tailoring properties in ferrite perovskite heterostructures", S. J. May, Telluride Workshop on Competing Interactions and Colossal Responses in Transition Metal Compounds, Telluride, CO, June 26-30, 2017.
10. "A strain mediated ferromagnetic to antiferromagnetic transition in ESMO thin films" S. Disseler, A. Grutter, E. J. Moon, D. Gilbert, E. Arenholz, and S. J. May. American Physical Society March Meeting, New Orleans, March 13 – 17, 2017.
11. "Probing tailored octahedral modulations in isovalent superlattices with standing-wave-excited angle-resolved photoemission" W. Yang, R. Chandrasena, E. J. Moon, A. Arab, V. Strokov, S. May, and A. Gray. American Physical Society March Meeting, New Orleans, March 13 – 17, 2017.
12. "Probing non-collinear magnetism in $Ca_{1-x}Sr_xMn_7O_{12}$ films by neutron scattering" A. Huon, A. Grutter, B. Kirby, S. Disseler, J. Borchers, Y. Liu, W. Tian, A. Herklotz, H. N. Lee, M. Fitzsimmons, and S. May. American Physical Society March Meeting, New Orleans, March 13 – 17, 2017.
14. "Epitaxial growth of $CaMn_7O_{12}$ thin films by both ozone-PLD and oxide MBE" A. Huon, H. N. Lee, and S. J. May. 21st American Conference on Crystal Growth and Epitaxy, Santa Fe, NM, July 31 – August 4, 2017.
15.* "Employing strain and heterostructuring to control electronic properties of transition metal oxides." Paul C. Rogge, Advanced Light Source Users Meeting, Berkeley, CA. October 4, 2017
16.* "Anion-based approaches to engineering functionality in perovskite oxide heterostructures", S. J. May, Carnegie Mellon University, Materials Science and Engineering seminar, October 27, 2017.
17.* "Ferrate heterostructures: From metal-insulator transitions to ionic functionality", S. J. May, Rutgers University, Institute for Advanced Materials, Devices, and Nanotechnology seminar, February 1, 2018.
18.* "Magnetism and electronic phase transitions in isovalent manganite and ferrate superlattices", S. J. May, American Physical Society March meeting, Los Angeles, CA, March 5-9, 2018.
19.* "Structural approaches for controlling magnetism and metal-insulator transitions in oxide heterostructures", S. J. May, University of Florida, Physics Department seminar, March 26, 2018.
20.* "Functional Properties of $CaFeO_3$ and $SrFeO_3$ Heterostructures", S. J. May, 5th Workshop on Complex Oxides, Capri, Italy, May 21-25, 2018.
21.* "Opportunities in magnetic oxide interfaces", S. J. May, Quantum Materials Young Investigators Workshop, Oak Ridge, TN, June 7-8, 2018.
22. "Orbital polarization in negative charge transfer ferrate perovskites" P. C. Rogge, R. J. Green, G. Fabbris, A. Barbour, A. Huon, H. N. Lee, P. Shafer, E. Arenholz, G. A. Sawatzky, M. P. M. Dean, and S. J. May, International Workshop on Oxide Electronics, Chicago, IL, September 25-27, 2017.
23. "Structure, magnetic, and electronic properties of epitaxial $Ca_{1-x}Sr_xMn_7O_{12}$ films" A. Huon, S. J. May, A. Grutter, J. Borchers, M. Fitzsimmons, and H. N. Lee, American Physical Society March meeting, Los Angeles, CA, March 5-9, 2018.
24. "Helical magnetic ordering in epitaxial $SrFeO_3$ and $CaFeO_3$ heterostructures", P. C. Rogge, R. J. Green, and S. J. May, International Conference on Magnetism, San Francisco, CA, July 16-20, 2018.

25.* “Metal-insulator transition, ligand holes, and orbital polarization in $CaFeO_3$ heterostructures”, S. J. May, Spin and Electronic Order in Functional Materials workshop at the Advanced Light Source user meeting, October 3 – 4, 2018.
26.* “Effect of strain on the metal-insulator transition and orbital polarization in strongly covalent $CaFeO_3$”, P. C. Rogge, Electronic Materials and Applications Conference, Orlando, FL, January 23 – 25, 2019.
27.* “Control of electronic bandwidth and hybridization in quantum oxide heterostructures”, S. J. May, University of Delaware seminar, September 17, 2018.
28.* “Anion-based approaches to engineering functionality in perovskite oxide heterostructures”, S. J. May, UC Davis, MSE seminar, October 2, 2018.
29.* “Anion-based approaches to engineering functionality in perovskite oxide heterostructures”, S. J. May, University of Michigan, MSE seminar, April 5, 2019.
30. “Incommensurate helical magnetism in epitaxial $SrFeO_3$ and $CaFeO_3$ heterostructures”, P. C. Rogge, R. J. Green, and S. J. May, Joint MMM-Intermag Conference, Washington, DC, January 14 – 18, 2019.
31. “Depth-profiling metal-oxygen hybridization and orbital polarization in isovalent perovskite oxide heterostructures”, Paul C. Rogge, Padraic Shafer, Gilberto Fabbris, Wen Hu, Elke Arenholz, Mark P. M. Dean, Steven J. May, American Physical Society March meeting, Boston, MA, March 4 – 8, 2019.
32. “Depth-resolved modulation of metal-oxygen hybridization and orbital polarization across isovalent oxide interfaces”, P. C. Rogge, P. Shafer, G. Fabbris, W. Hu, E. Arenholz, E. Karapetrova, M. P. M. Dean, R. J. Green, and S. J. May, International Workshop on Oxide Electronics, Kyoto, Japan, Sept. 30 – Oct. 2, 2019.
33.* “Control of electronic character in oxide heterostructures: Beyond charge-based doping”, S. J. May, Temple University, physics colloquium, October 28, 2019.
33.* “Depth-profiling electronic degrees of freedom in epitaxial heterostructures with resonant soft x-ray reflectivity”, S. J. May, NSLS II user meeting, Soft X-ray Scattering and Spectroscopy at NSLS-II: Gap Analysis workshop, May 18-20, 2020 (held virtually).
34.* “Probing electronic degrees of freedom at buried interfaces in quantum heterostructures using resonant x-ray reflectivity”, S. J. May, Electronic Materials Conference, June 24-26, 2020 (held virtually).
35.* “Effect of interfaces on band hybridization, orbital polarization, and helical magnetism in $SrFeO_3/CaFeO_3$ heterostructures”, S. J. May, American Physical Society March meeting, March 15-19, 2021 (held virtually).